THE INVERSE PROBLEM OF ELECTROCARDIOGRAPHY - INCREASING THE STABILITY BY USING A SIMPLIFIED GEOMETRY FOR THE ISCHEMIC REGION

OLE LØSETH ELVETUN

NORWEGIAN UNIVERSITY OF LIFE SCIENCES
DEPARTMENT OF MATHEMATICAL SCIENCES AND TECHNOLOGY
MASTER THESIS 60 CREDITS 2011

Abstract

We aim to obtain stability when using ECG recordings, the bidomain model and lab measurements to locate an ischemic region in the heart. Historically, this has proven to be a difficult task when using a general geometry, so our approach is to assume a priori that we can approximate the ischemic region as a ball.

The approximation has been viewed from both a theoretical stand as well as more practically with numerical simulations. First, the theoretical continuity properties of the system with the simplified geometry were explored, followed by several numerical simulations to illuminate the practical behavior with this geometry.

We did find a theoretical stability, as well as promising numerical results. From a small compact domain of the heart, we have proved a continuous inverse. In addition, we found a necessary demand for uniqueness of the inverse solution throughout the entire heart – which then also guarantee continuity. Numerically, we were able to retrieve the ischemic region without noise as well as with a proper amount of noise on our synthetic forward data.

These findings are interesting to pursuit further. Since we worked on synthetic data in this thesis, it will be of great importance to further work with true patient data to see how well we can approximate the ischemic region in a real case. Also, the key point of this thesis was to gain more stability. In theory we found this to be stable, but we do not know *how* stable it is when it comes to numerical simulations. It might therefore be interesting to try to determine how sensitive the numerics can be to noise.

Contents

Preface

This thesis marks the end of my master degree at the Norwegian University of Life Sciences. When starting this voyage, around five years ago, I did not know that applied mathematics would be my destination. As a freshman, I did in fact start out as an engineering student. However, during the basic courses, my interest for mathematics grew, and the final push to pursuit this path was given to me during an exchange period at the University of British Columbia, where I truly learned to appreciate this field. The systematic way to explore the world is what I find so appealing about mathematics.

Along the way there have been many people to thank for helping me, both directly and indirectly.

Of course, a great thanks goes to my supervisor Bjørn Fredrik Nielsen, for always having the time to discuss problems I have encountered during my thesis, as well as having challenged me to reach a higher level of mathematical understanding during my work. Also, the rest of the mathematical section at the institute have my gratitude for always having their doors open to my questions during all my years at the university, both as their student and as their teaching assistant.

The great environment in the reading room is also to be thanked. The people in this room has been the source of many interesting and funny discussions as well as many welcoming coffee breaks.

A somewhat special thanks should be given to my brother - the medicine student - for bringing his 10kg physiology book home to my parents on holidays so I could read myself up on the field over the summer.

Finally I would like to thank my family for giving me love and support during all these years, and my girlfriend for being so understanding and supportive during my work.

Ole Løseth Elvetun Ås, Norway.

1 Introduction

A problem in mathematical biology that's been under heavily inspection the last decades, is the inverse problem of electrocardiography. Namely, can we locate a region in the heart experiencing an early phase of a heart attack – an ischemic region – from a recorded electrocardiogram? In 1988 the findings were summarized in the articles [16, 17, 18, 19, 20]. At this stage, however, the results were very unreliable, in the sense that they were highly unstable. The problem was partially dealt with using some form of regularization, like Tikhonov regularization. This only gave some success, so much effort has been put into the field since, to achieve better results. In the summarizing article [21], the authors describe the two main paths to handle this: Either to reduce the error sources of the problem or try to incorporate more a priori information about the problem.

Even though these methods have given some results, it is still hard to overcome the instability. One reason for this is due to that people have heavily focused on the mathematically side of the problem, trying to solve this for a general geometry of the ischemic region. In the end, however, the user of the information mathematicians can retrieve from the electrocardiogram, will be cardiologists. They want to decide where the blocking in one of the coronary arteries is located.[1] When mathematicians try to model this with a general geometry, they have to use a regularization, even after all the initial assumptions made when deriving the model. Therefore, we suggest another approach. Instead of trying to find a very sophisticated geometry for the ischemic region with the help of regularization, we assume a simple geometry a priori. Then we use this geometry, e.g. a ball, when we try to retrieve an ischemic region from the electrocardiogram.

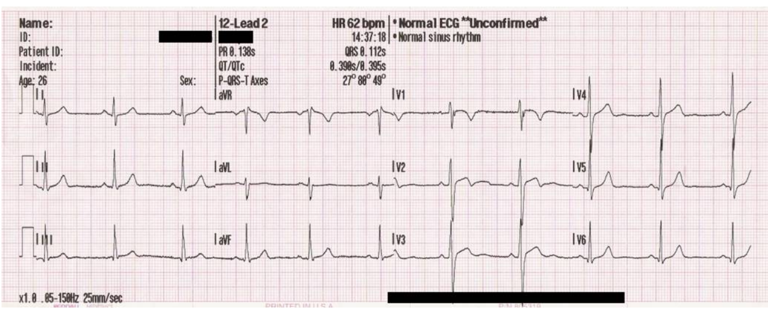

Figure 1: A traditional ECG reading of a 26 year old male, using 12 electrodes. Picture taken from Wikipedia.

[1] A coronary artery is an artery providing blood to the heart itself.

This first chapter will give a quick introduction to the entire problem. First, we will introduce those not very familiar to the cardiovascular system to this field, before showing the reader how we physically can justify the bidomain model, and then further how mathematical theory combined with lab results from medicine can be used to modify the bidomain model to get the a single partial differential equation useful for computing the extracellular potential in the body. It is then natural to discuss the existence and uniqueness of this PDE, before we give a brief illumination of what we are going to do throughout the main part of this thesis; how to find the ischemic region from the recorded electrocardiogram, whether a least-squares solution exists, if it is unique and if it depends continuously on the data, and what additional requirements we might have to impose to get these properties.

1.1 The cardiovascular system

Located in the chest cavity, the heart is a pump running the human circulation. In fact, is consists of two pumps – the left-sided and the right-sided heart. The right-side is running the pulmonary circulation, which is pumping oxygen depleted blood to the lung. Returning blood enters the systemic circulation, sending blood through the rest of the body through the aorta. These two main circuits is called the vascular system. Both pumps consist of an atrium and a ventricle, where the atria are the chambers receiving blood and the ventricles are discharging blood [23].

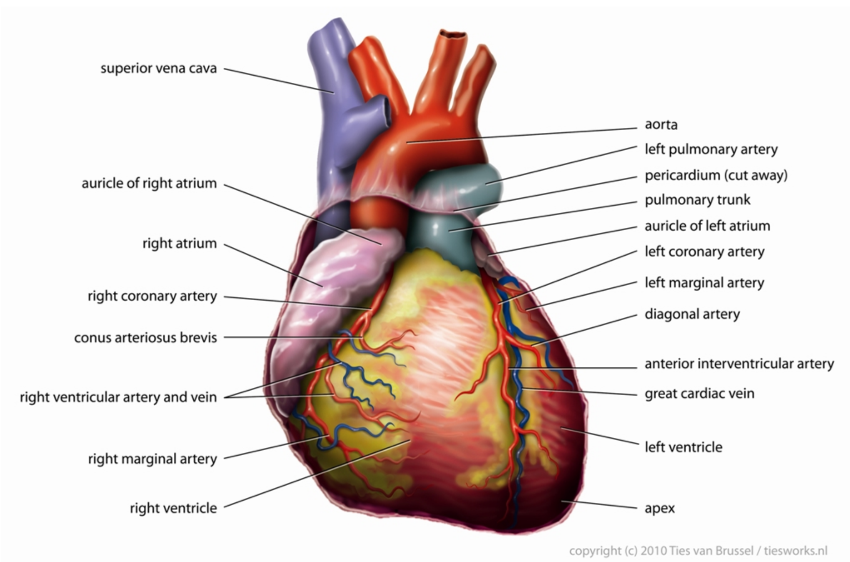

Figure 2: The human heart. Picture is from Wikipedia, by Ties van Brussel

As a full phase, the blood enters the right atrium through the superior vena cava, before being pumped through the tricuspid valve into the right ventricle. From here, is goes through the pulmonary value into the pulmonary arteries. After running though the lungs, the blood comes back through the pulmonary veins into the left atrium, before it enters the left ventricle after being pumped through the mitral valve. Then it leaves through the aortic value to the aorta before entering the systemic circulation [22].

But for this fine system to work there must be something triggering the pump. In fact, all cardiac cells are electrically active, originating from a group of cells in the right atrium depolarizing simultaneously. From here, the electrical signal spreads like a wave through the entire heart making the heart contract. The timing must be perfect for optimizing the blood flow.

As mentioned, this starts from a group of cells in the right atrium. More precisely the sinoatrial(SA) node. Roughly 100 ms after firing, the potential reaches the atrioventricular(AV) node. Because of the atrioventricular ring, the impulse does not go directly from the atria to the ventricles, but instead have to take the way to the His-Purkinje fiber system. This is a network of specialized conductive cells carrying the signal to the muscles of both ventricles [23].

In total there are five phases in what is called the cardiac action potential[3], describing how the electrical potential of a cell in the heart changes. Depending on location in the heart, the initialization, shape and duration of this action potential differs, because of different channels and anatomy of different myocytes – muscle cells.

Despite these differences, we have strong similarities, and thus we can as mentioned speak of five phases, although the SA and AV node only have three of these present.

Phase four, which is the resting phase, corresponding to the diastolic(filling) phase of the heart, is the natural state, and a cell will remain in this state until it receives an external stimulus from adjacent cells.

Phase zero follows – the rapid depolarization phase, when a cell opens the Na^+ and Ca^{2+}-channels, and the potential rapidly rises due to rapidly flow of such ions into the cell. However, in the SA and AV-node we will only have Ca^{2+}-channels, leading to a slower upstroke, since these channels are slower. These nodes will not experience the two next phases either.

Phase one is the rapid repolarization, where the Na^+-channels gets mostly inactivated together with the activation of a outward K^+-current.

Phase two is the plateau phase, where there is a balance between the inward Na^+-channel and the outward K^+-channel, leading to basically no net flow.

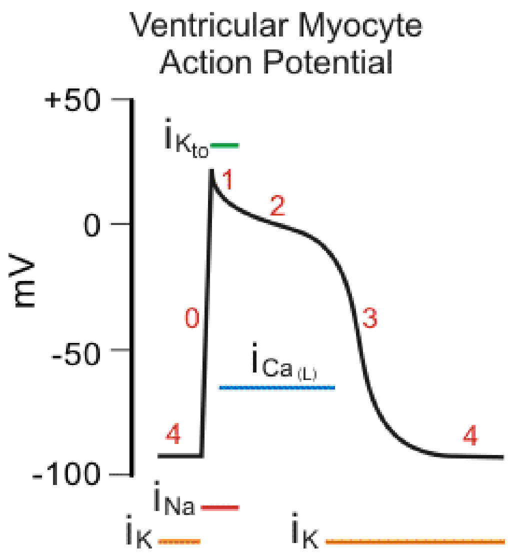

Figure 3: The action potential for the myocardium. Picture is from cvphysiology.com, by R. E. Klabunde, Ph.D.

Phase three follows. This is known as the repolarization phase, when the outward channels remains open, but the Ca^{2+}-channels close, and hence we get a decrease in potential.

Having described the steps of the process, we have yet to explain how to get back to the resting phase. The answer to this is the pacemaker current, also known as the funny current, present in the SA node, the AV node as well as in the Purkjine fibers of the heart. This current is routed along a cation channel called HCN(hyperpolarization activated, cyclic nucleotide gated). At the end of phase three, the channel is activated by hyperpolarization. This happens as the membrane potential gets below the threshold for the HCN channel, starting a slow depolarizing current. Then, the Ca^{2+}-channels gets activated by the beginning depolarization as a result from the funny current [23].

We know the geometry of the heart and how it beats by now. For the heart to be able to beat, of course the heart muscle – the myocardium – needs blood itself. The arteries for this job is called coronary arteries. These arteries, named the left and right coronary artery, originates from the root of aorta, before splitting into smaller branches later. When one of the coronary arteries narrows due to atherosclerosis, which is a condition where cholesterol and other materials extends the artery wall, the patient has what is known as ischemic heart disease [2]. In the early stages this is a reversible condition, but if however it evolves and results in a full blockade of the artery, the affected part of the heart dies as the patient experiences a heart attack.

To determine whether a patient has ischemic heart disease, it is common to inject a radioactive isotope into the blood system and expose the patient for physical stress, and then measure possible accumulation of the injected isotope in the ischemic region. This is, however, an expensive and time-consuming method, so the goal by the inverse ECG is to diagnose this by simple ECG measurements and mathematical methods.

1.2 Physical interpretation of the bidomain model

The bidomain model was first introduced in 1969 [27] before it was mathematically formulated in 1978 [28], and it is used to model the electrical activity of the heart.

In the bidomain model, the space inside the cells is called the intracellular domain, and the space between the cells is called the extracellular domain, separated by a membrane. This applies only inside the heart. Outside the heart, i.e in the torso, we have only a single domain, corresponding to the extracellular domain in the myocardium. This is due to the fact that inside the heart we are interested in the active cells, in contrast to the torso, which we only consider as a passive conductor [1]. By defining the potential difference across the cell membrane as $v = u_i - u_e$, where u_i and u_e are the intracellular and extracellular potentials, the bidomain model can be derived. Ohm's law states that

$$\mathbf{J} = \frac{1}{R}\mathbf{E}, \tag{1.1}$$

where $\mathbf{J}$ is the current density, $\mathbf{E}$ is the electric field strength, and R is the resistivity. From electrostatic, the electric field can be expressed as the negative gradient of the potential, and the conductivity, M, is defined as the reciprocal of the resistivity. Hence we get

$$\mathbf{J}_i = -M_i \nabla u_i, \text{ and} \tag{1.2}$$

$$\mathbf{J}_e = -M_e \nabla u_e. \tag{1.3}$$

The electric fields in the heart is not stationary. However, the changes are relatively slow, so making this assumption is fair enough. If the heart is considered in isolation, it follows that current leaving one of the domains must enter the other, since we assume no accumulation of charge. Hence, the change in current density must be equal in magnitude and opposite in sign. Also, we assume no current flow from the intracellular region to the torso, and all flow from the extracellular region to the torso are govern by some specific boundary conditions which we will return to in the next section. Mathematically, we now have

$$-\nabla \cdot \mathbf{J}_i = \nabla \cdot \mathbf{J}_e, \tag{1.4}$$

which we can combine with (1.2) and (1.3) to obtain

$$\nabla \cdot (M_i \nabla u_i) = -\nabla \cdot (M_e \nabla u_e). \tag{1.5}$$

Furthermore, by subtracting $\nabla \cdot (M_i \nabla u_e)$ from both sides, we get

$$\nabla \cdot (M_i \nabla u_i) - \nabla \cdot (M_i \nabla u_e) = -\nabla \cdot (M_e \nabla u_e) - \nabla \cdot (M_i \nabla u_e). \tag{1.6}$$

At last, remember the definition of the potential difference across the cell membrane. By applying this, the bidomain equation becomes

$$\nabla \cdot (M_i \nabla v) = -\nabla \cdot ((M_i + M_e)\nabla u_e). \tag{1.7}$$

Actually, the bidomain model consists of one more PDE along with a system of ODEs, modeling the ionic channels, to get a closed system. Since these are of no interest in this thesis, we will not state them here.

1.3 Mathematical derivation of the PDE

As we have explained earlier, there are five phases in the cardiac action potential. Even though that was at the cell level, there will be points in time when all cells are at the resting phase and at the plateau phase simultaneously. This fact will be of utter importance to the mathematical model we are going to derive. But first, let us just rewrite the bidomain model and define all the involved parameters.

$$\nabla \cdot (M_i \nabla v) + \nabla \cdot ((M_i + M_e)\nabla u_e) = 0 \;\; in \; H, \tag{1.8}$$

where

- M_i and M_e are the intracellular and extracellular conductivities,
- H is the domain of the heart (We will later introduce T for torso and B for body),
- v is the transmembrane potential,
- u_e is the extracellular potential.

As mentioned, there are two phases during a heart beat for which the entire heart is in the same state, the plateau and the resting phase, denoted by t_1

and t_2 respectively. Lab measurements have provided data for the potentials during these states [2],

$$v(x,t_1) \approx \begin{cases} 20mV, \text{ x in healthy tissue,} \\ -20mV, \text{ x in ischemic tissue,} \end{cases} \tag{1.9}$$

and

$$v(x,t_2) \approx \begin{cases} -80mV, \text{ x in healthy tissue,} \\ -70mV, \text{ x in ischemic tissue.} \end{cases} \tag{1.10}$$

Now, we can define a new variable h by

$$h(x) = v(x,t_1) - v(x,t_2) \approx \begin{cases} 100mV, \text{ x in healthy tissue,} \\ 50mV, \text{ x in ischemic tissue.} \end{cases} \tag{1.11}$$

This is called the shift in the transmembrane potential, and likewise we will define the shift in the extracellular potential as

$$r(x) = u_e(x,t_1) - u_e(x,t_2). \tag{1.12}$$

The equation (1.8) must hold for any t, so clearly it holds for t_1 and t_2, thus subtracting the equation at time t_2 from the equation at time t_1, gives

$$\nabla \cdot ((M_i + M_e)\nabla r) = -\nabla \cdot (M_i \nabla h) \text{ in } H. \tag{1.13}$$

In the torso, the cells are relatively non-active. So in this model, we assume that these cells do not change their electric properties, allowing the modeling error regarding active cells in the torso. For instance, muscle cells contracts due to change in electrical potential. However, we can now model the torso as a passive conductor. Mathematically, this can be described by the following homogeneous elliptic PDE:

$$\nabla \cdot (M_o \nabla r) = 0 \text{ in } T. \tag{1.14}$$

Furthermore, it is assumed that the body is insulated. Mathematically, this means that there is no flux over the boundary of the body, which can be expressed as follows with a formula from basic calculus

$$(M_o \nabla r) \cdot \mathbf{n_b} = 0, \; x \in \partial B, \tag{1.15}$$

where B is defined by $B = \bar{\text{H}} \cup T$. In addition, conditions at the interface between H and T are required [24]:

$$\begin{aligned} r_H &= r_T \; on \; \partial H, \\ (M_e \nabla r_H) \cdot \mathbf{n_H} &= -(M_o \nabla r_T) \cdot \mathbf{n_T} \; on \; \partial H, \\ (M_i \nabla h + M_i \nabla r_H) \cdot \mathbf{n_H} &= 0 \; on \; \partial H. \end{aligned} \tag{1.16}$$

Moving on from the assumptions, we can now derive the weak formulation of the PDE, so first we will multiply the left-hand side of equation (1.13) by $\psi \in C^\infty(B)$, and integrate by parts over H to derive

$$\begin{aligned}&\int_H \psi\nabla\cdot((M_i+M_e)\nabla r)dx \\ &\quad = -\int_H \nabla\psi\cdot((M_i+M_e)\nabla r)dx + \int_{\partial H}\psi((M_i+M_e)\nabla r)\cdot\mathbf{n_H}dS, \end{aligned} \tag{1.17}$$

by applying Gauss-Green's theorem. Likewise, we can do the same for the right-hand side, and get

$$-\int_H \psi\nabla\cdot(M_i\nabla h)dx = \int_H \nabla\psi\cdot(M_i\nabla h)dx - \int_{\partial H}\psi(M_i\nabla r)\cdot\mathbf{n_H}dS. \tag{1.18}$$

By following the same strategy, we get an expression from equation (1.14) which reads:

$$\int_T \psi\nabla\cdot(M_o\nabla r) = -\int_T \nabla\psi\cdot(M_o\nabla r) + \int_{\partial H}\psi(M_o\nabla r)\cdot\mathbf{n_T}dS. \tag{1.19}$$

Note that the integral over the boundary only includes the boundary at the heart, since from equation (1.14), we get that the rest of the integral is equal to zero. Now, by combining (1.17)-(1.19), and imposing the conditions (1.16), given at the interface between H and T, we get

$$\int_B \nabla\psi\cdot(M\nabla r)dx = -\int_H \nabla\psi\cdot(M_i\nabla h)dx, \tag{1.20}$$

where

$$M = \begin{cases} M_i + M_e & \text{for x} \in \text{H}, \\ M_o & \text{for x} \in \text{T}. \end{cases}$$

By a density argument, the class of test functions can be extended, so the above weak formulation of the PDE will hold for any $\psi \in H^1(B)$, where $H^1(B) = \{u \in L^2(B) : \nabla u \in L^2(B)\}$. Note that the right-hand side of (1.20) is known due to the lab results summarized in (1.11).

1.4 Existence and uniqueness

The PDE from (1.20) won't provide a unique solution, since the function itself is not a part of the PDE, but only it's derivative, this also applying to the boundary condition (1.15). If some function r $\in H^1(B)$ is a solution, then r + c, where c is an arbitrary constant, will also be a solution. Hence, we ought to search for a solution in a different space. Common practice in Sobolev space theory is to search for a solution in the space

$$X = \left\{ u \in H^1(B) \,\middle|\, \int_B u = 0 \right\}, \tag{1.21}$$

with the norm inherited from $H^1(B)$. Then, our problem reads: Find $r \in X$ such that

$$\int_B \nabla\psi \cdot (M\nabla r)dx = -\int_H \nabla\psi \cdot (M_i \nabla h)dx, \quad \forall \psi \in X. \tag{1.22}$$

To show existence, we will first consider the bilinear form associated with this PDE, and prove that this is continuous. This bilinear form $\hat{L}(\cdot,\cdot) : X \times X \longmapsto \mathbb{R}$ is defined by

$$\hat{L}(r,\psi) = \int_B \nabla\psi \cdot (M\nabla r)dx. \tag{1.23}$$

The objective of introducing this bilinear operator is to use it to prove existence and uniqueness, by showing that it is symmetric, continuous and coercive, and therefore forms an equivalent inner product on X (Proof 4 - Appendix A). If so, we can use Riesz' representation theorem, which states an important fact between a Hilbert space and its dual space; they are isometrically isomorphic. More formally, this can be written as:

Riesz' representation theorem - Let H be a Hilbert space with an inner product $(\cdot,\cdot)$. For any linear functional $f : H \longmapsto \mathbb{R}$, there exists a unique element $u \in H$ such that

$$f(v) = f_u(v) = (u,v), \quad \forall v \in H. \tag{1.24}$$

and

$$\|f_u\|_{H^*} = \|u\|_H. \tag{1.25}$$

The mapping $u \mapsto f_u$ is a linear isomorphism of H onto H^*[4, 8]. Hence, the Hilbert space is identified with its dual space in sense of the norm.

If we go back to (1.22), and define the linear functional $\hat{Q}_h : X \longmapsto \mathbb{R}$ as

$$\hat{Q}_h(\psi) = -\int_H \nabla\psi \cdot (M_i \nabla h)dx, \tag{1.26}$$

we can define our problem(1.22) on a more abstract form as: Find $r \in X$ such that

$$\hat{L}(r,\psi) = \hat{Q}_h(\psi), \quad \forall \psi \in X. \tag{1.27}$$

Now, since $\hat{Q}_h$ is a linear functional, we will have a unique element in X identified with this linear functional, from Riesz' representation theorem. Thus, if we can show the attributes of $\hat{L}(\cdot,\cdot)$ as mentioned above, we will have a unique solution to the problem. But, we will first state the requirements on the conductivities. They must be symmetric and strictly positive definite, i.e

$$x^T M(x)x \geq \Theta|x|^2, \ \forall \ x \in \mathbb{R}^3, \ \Theta > 0, \tag{1.28}$$

where Θ is constant. From this, we can start to show our claims. Symmetry follows from

$$\hat{L}(r,\psi) = \int_B \nabla\psi \cdot (M\nabla r)dx = \int_B (M^T\nabla\psi)\cdot\nabla r dx$$
$$= \int_B (M\nabla\psi)\cdot\nabla r dx = \hat{L}(\psi, r). \quad (1.29)$$

The next step is to show continuity:

$$|\hat{L}(r,\psi)| = \left|\int_B \nabla\psi\cdot(M\nabla r)dx\right| \le \int_B |\nabla\psi\cdot(M\nabla r)|dx$$
$$\le \int_B |M_{11}r_{x1}\psi_{x1}| + |M_{12}r_{x2}\psi_{x1}| + ... + |M_{33}r_{x3}\psi_{x3}|dx$$
$$\le \sup|M_{11}|\|r_{x1}\|_{L^2(B)}\|\psi_{x1}\|_{L^2(B)} + ... \le C\|r\|_X\|\psi\|_X. \quad (1.30)$$

by Hölder's inequality. Thus, the bilinear form is continuous, since we have equivalence between boundedness and continuity for linear operators [8]. To show the last claim, coercivity, we need the inequality [4]:

Poincarè's inequality - Let $U \subset \mathbb{R}^n$ be a bounded, connected, open set. Then there exists a constant C, such that

$$\|u-\bar{u}\|_{L^2(U)} \le C\|\nabla u\|_{L^2(U)}, \ \forall\ u \in H^1(U), \quad (1.31)$$

where $\bar{u}$ denotes the average of the function over the domain, i.e

$$\bar{u} = \frac{1}{|B|}\int_B u\ dx. \quad (1.32)$$

Note, however, that in our space, we have an average of zero. Hence, we can use the inequality (1.31) to derive

$$\|r\|^2_{H^1(B)} = \|r\|^2_{L^2(B)} + \|\nabla r\|^2_{L^2(B)} \le (C^2+1)\|\nabla r\|^2_{L^2(B)}. \quad (1.33)$$

Now, by using the fact that $M(x)$ is positive definite, we can furthermore show that

$$\hat{L}(r,r) = \int_B \nabla r\cdot M\nabla r\ dx = \int_B (\nabla r)^T M\nabla r\ dx$$
$$\ge \int_B \Theta|\nabla r|^2\ dx = \Theta\|\nabla r\|^2_{L^2(B)}. \quad (1.34)$$

Thus, it follows that

$$\|r\|^2_{H^1(B)} \le \frac{C^2+1}{\Theta}\hat{L}(r,r), \quad (1.35)$$

meaning that $\hat{L}(\cdot,\cdot)$ is coercive, and together with the symmetry and continuity properties, the bilinear operator is an equivalent inner product on X. Now, we use the Riesz representation theorem explained earlier. Then, we know that there exists a unique $g \in X$ such that

$$\hat{L}(g,\psi) = \hat{Q}_h(\psi), \quad \forall \psi \in X. \tag{1.36}$$

We then obtain $r = g$.

By now, we have a solution in $H^1(B)$ when we know the shift in the extracellular potential (1.11). The electrocardiogram is only recorded on the boundary of the body. Hence, we still need to be sure we are able to assign "boundary values" to this function. Luckily, from Sobolev space theory[4] we have

The trace theorem - For any bounded region U, with a C^1-boundary, there exists a bounded linear operator

$$T : H^1(U) \to L^2(\partial U), \tag{1.37}$$

such that

$$\|Tu\|_{L^2(\partial U)} \leq C\|u\|_{H^1(U)}, \forall u \in H^1(U). \tag{1.38}$$

Note, however, that this does not imply that we can assign values in a pointwise sense, since L^2 does not provide us any information on sets of measure zero. What this theorem merely says, is that we can think of the restriction $u|_{\partial U}$ of some function $u \in H^1$ as a $L^2(\partial U)$-function.

To sum up, *the forward problem* consists of taking the shift h(1.11) in the extracellular potential(and by that, the ischemic region), and find a solution - r of (1.22) - in $H^1(B)$ before using the trace operator to find a function defined on the surface of the body. More details of representing the ischemic region will be discussed thoroughly in the next section.

1.5 The inverse problem

If we have strictly positive definite conductivities, and search in the right space, we will have a unique solution of the forward problem. But as explained in the introduction, our goal is to find the inverse solution, that is, to find the domain D in the heart which contains the ischemic tissue, i.e

$$D = \{x \in H | h(x) \approx 50mV\}, \text{ (see (1.11))}. \tag{1.39}$$

The idea of how to do this, is to use the electrocardiogram, which is a recording of the electrical activity of the heart - or in mathematical terms a mapping from the surface of the body to the real numbers, along with the assumption that we could use a sphere to approximately represent the ischemic region. The electrocardiogram and our approximation assumption turn our problem into finding the spherical coordinates (x_0, y_0 and z_0) for the center of the sphere and the radius (s), which in turn should represent the ischemic region (1.39). By introducing the cost-functional $J : \mathbb{R}^4 \longmapsto \mathbb{R}$ defined by

$$J(x_0, y_0, z_0, s) = \frac{1}{2} \int_{\partial B} (r(x_0, y_0, z_0, s) - d)^2 \, dS, \tag{1.40}$$

the problem reads:

$$\min_{x_0, y_0, z_0, s} J(x_0, y_0, z_0, s), \tag{1.41}$$

subject to

$$\int_B \nabla\psi \cdot (M\nabla r) dx = -\int_H \nabla\psi \cdot (M_i \nabla h(D)) dx \;\; \forall \; \psi \in X. \tag{1.42}$$

The solution to the forward problem is depending on the center and the radius of the ischemic region in the sense that h, the shift in the transmembrane potential, takes different values regarding if we are inside or outside the ischemic region (1.39).

Now, to find an expression for the ischemic domain, first remember that the values the shift in the transmembrane potential takes in the ischemic and the healthy region of the heart is known(1.11). By introducing the Heavside function, which reads

$$G(x) = \begin{cases} 1, & x > 0, \\ 0, & x < 0, \end{cases} \tag{1.43}$$

we can express the shift, h, as the function

$$h(\phi) = 50(1 - G(\phi)) + 100G(\phi), \tag{1.44}$$

where ϕ is a function which takes negative values inside the ischemic region, zero on the boundary and positive values in the rest of the heart, and G is the Heavside function just introduced in (1.43). However, G is a discontinuous function, but research suggests that the transition is smooth, hence the use of an approximated Heavside function is common. We will use an approximated Heavside function previously used by a research team at Simula[2], which reads

$$G_\tau(\phi) = \begin{cases} 0, \text{ if } \phi < -\tau, \\ 1, \text{ if } \phi > \tau, \\ \frac{1}{2}\left[1 + \frac{\phi}{\tau} + \frac{1}{\pi}\sin\left(\frac{\pi\phi}{\tau}\right)\right], \text{ if } |\phi| \le \tau. \end{cases} \tag{1.45}$$

Further, we need an expression for the ϕ-function. We have already mentioned the requirements; negative values inside the ischemic region and positive outside. In 2D, the function

$$\phi(x, y) = (x - x_0)^2 + (y - y_0)^2 - s^2, \tag{1.46}$$

where (x_0, y_0) is the center of the ischemic region, and s is the radius, will satisfy these requirements. This is an easy choice, and it can also easily be extended to 3D or restricted to 1D by adding z or removing y, respectively. In the bidomain model, clearly the gradient of h is zero if $|\phi| > \tau$, since G_τ is constant in this region. So, the only area for which there is a gradient different from zero, is in the transition zone, where $|\phi| \leq \tau$. This gradient can be calculated using the chain rule

$$\nabla h(\phi(x)) = h'(\phi)\nabla\phi(x), \tag{1.47}$$

which gives us the following expression for ∇h

$$\nabla h(\phi(x)) = \begin{cases} \frac{50}{\tau}\left(1 + cos\left(\frac{\pi\phi}{\tau}\right)\right)(\vec{i}(x - x_0) + \vec{j}(y - y_0)) \text{ if } |\phi| < \tau, \\ 0 \text{ elsewhere.} \end{cases}$$

Hence we have an expression for the gradient of the transmembrane potential. But it remains to show how this can be used to find the ischemic region. To do so, let us first consider the bidomain model again(1.27).

$$\hat{L}(r, \psi) = \hat{Q}_h(\psi). \tag{1.48}$$

To work with this equation any further in this section will be cumbersome. Hence, we will introduce the linear operators associated with this PDE. We introduce $L : X \longmapsto X^*$ and $Q : X \longmapsto X^*$ by

$$\langle Lr, \psi\rangle = \hat{L}(r, \psi) \tag{1.49}$$

and

$$\langle Qh, \psi\rangle = \hat{Q}_h(\psi), \tag{1.50}$$

where these right-hand sides are the expression from the PDE (1.27), and $\langle\cdot, \cdot\rangle$ denotes the pairing between X^* and X. From Riesz' representation theorem, we then have that for any $\hat{Q} \in X^*$, there exists a unique $r \in X$ such that

$$\langle Lr, \psi\rangle = \hat{L}(r, \psi) = \hat{Q}(\psi), \quad \forall\psi \in X, \tag{1.51}$$

and

$$\|Lr\|_{X^*} = \|r\|_X. \tag{1.52}$$

In other words, the mapping $L : X \longmapsto X^*$ is a isometric isomorphism of X onto X^*. Hence, we know that L has an inverse. This means that we can write our equation on the form

$$Lr = Qh(\phi) \tag{1.53}$$

$$\Rightarrow r = L^{-1}Qh(\phi). \tag{1.54}$$

When we go back to look at the inverse problem, this new syntax is easier to work with. Our goal was to minimize the cost-functional from eq (1.40), but this was connected to the solution of the partial differential equation(1.42). Hence, we need to introduce the Lagrangian, and we get

$$\mathcal{L}(x_0, y_0, s, \lambda) = J(x_0, y_0, s) - \lambda(Lr - Qh(x_0, y_0, s)). \tag{1.55}$$

Now, we can incorporate the first-order optimality condition, which states that the gradient of the Lagrangian should equal zero. That is

$$\nabla\mathcal{L}(x_0, y_0, s, \lambda) = \nabla J(x_0, y_0, s) - \nabla\lambda(Lr - Qh(x_0, y_0, s)) = 0. \tag{1.56}$$

where

$$\nabla = \left(\frac{\partial}{\partial x_0}, \frac{\partial}{\partial y_0}, \frac{\partial}{\partial s}, \frac{\partial}{\partial \lambda}\right). \tag{1.57}$$

Note that when we set the derivative with respect to λ equal to zero, we get back the constraint govern by the PDE in (1.53). We need to compute the derivatives of the cost-functionals. To do so, let us start with the derivative with respect to x_0:

$$\begin{aligned}
\frac{\partial J}{\partial x_0} &= \frac{\partial}{\partial x_0}\int_{\partial B}\frac{1}{2}(TL^{-1}Q\{h(\phi(x_0, y_0, s))\} - d)^2 dS \\
&= \int_{\partial B}\left(TL^{-1}Q\{h(\phi(x_0, y_0, s))\} - d\right)\frac{\partial}{\partial x_0}\left(TL^{-1}Q\{h(\phi(x_0, y_0, s))\}\right) dS \\
&= -2\int_{\partial B}(TL^{-1}Q\{h(\phi(x_0, y_0, s))\} - d) \\
&\qquad (TL^{-1}Q\{h'(\phi(x_0, y_0, s))(x - x_0)\})dS.
\end{aligned} \tag{1.58}$$

The expression for $\frac{\partial J}{\partial y_0}$ is similar, when we substitute x_0 with y_0, and at last, the derivative with respect to s is

$$\begin{aligned}
\frac{\partial J}{\partial s} = -2\int_{\partial B}&(TL^{-1}Q\{h(\phi(x_0, y_0, s))\} - d) \\
&(TL^{-1}Q\{h'(\phi(x_0, y_0, s))s\})dS.
\end{aligned} \tag{1.59}$$

We now have shown how we can take the derivative with respect to all the variables in the minimization problem. Note that since T, L and Q are linear, the derivative does not affect any of these. The optimality system reads:

$$\begin{aligned}
\frac{\partial}{\partial x_0}J(x_0, y_0, s) - \frac{\partial}{\partial x_0}\lambda(Lr - Qh(x_0, y_0, s)) &= 0, \\
\frac{\partial}{\partial y_0}J(x_0, y_0, s) - \frac{\partial}{\partial y_0}\lambda(Lr - Qh(x_0, y_0, s)) &= 0, \\
\frac{\partial}{\partial s}J(x_0, y_0, s) - \frac{\partial}{\partial s}\lambda(Lr - Qh(x_0, y_0, s)) &= 0, \\
Lr - Qh(x_0, y_0, s) &= 0.
\end{aligned} \tag{1.60}$$

This problem might be solved with a “one-shot” method. However, this will not be done here. Instead, we will try to solve this optimality system using a numerical iteration method. The idea is to first guess a solution of the ischemic region. We then solve the forward problem with this ischemic region. Then, taking this solution, we find the gradient of the cost-functional, and use this to make a new guess for the ischemic region. For a more lucid explanation, see the iteration procedure below.

Algorithm 1 Landweber iteration

Make an initial guess $\tilde{x}_0$, on location and size of the ischemic region
repeat
    Solve $r_{k+1} = L^{-1}Qh(\phi(\tilde{x}_k))$
    Update the guess by $\tilde{x}_{k+1} = \tilde{x}_k - \beta\nabla J(r_{k+1})$
until $\|\tilde{x}_{x+1} - \tilde{x}_k\| < TOL$

1.6 Highlighting important topics

Following this quick introduction to the problem we face, we would like to give some more details around some of the important problems we will encounter throughout this thesis.

One of the main topics to investigate is the forward operator. This operator takes the ischemic parameters and maps them to electrical potentials recorded on the surface of the body. In the end, we would like to determine if the inverse of this operator is stable, but we will first consider the stability of the forward operator, as well as the cost-functional (1.40), since this might help us to determine the stability of the inverse operator. Therefore, we introduce a theorem:

Weierstrass' theorem - If f is a continuous, real-valued function on a non-empty compact set, then f will take a minimum value on this set.

Using this theorem, we know that the cost-functional has a minimum whenever the forward operator is continuous, since the cost-functional is continuous when the forward operator is (Proof 5 - Appendix A). We only require that the set of ischemic parameters is compact.

The next question that arises is whether we can find the inverse solution. Since we want to take a recorded electrocardiogram and go backwards, trying to find the ischemic region, we need to apply the inverse operator, and therefore the question concerning existence of an inverse operator is very important. Also, we would like for this inverse operator to be continuous, since we want small differences in measured potential to give small changes in the ischemic region. That is, to make it robust for noise or other anomalies.

In addition, the uniqueness of the least-squares solution is of major interest. When the true ischemic region has the shape of a sphere, we can use the inverse of the forward operator, but the true ischemic region will most likely have a shape different from a perfect sphere. Therefore, we will have to find the minimum of the cost-functional (the least-squares solution), and the continuity of this operation is important.

Numerically, we want to work with a convex set. As we will see in Chapter 2, there might be a problem with continuity of the least-squares solution when the set is non-convex. We mentioned above that we could choose a convex domain, but in the end of Chapter 2, it will be apparent that we need linearity to preserve convexity in the image. We will see shortly that our forward operator is non-linear, so the non-convexity will play a major part during the remaining part of this thesis. To see why the forward operator is non-linear, let us first discuss the mapping from the ischemic region to the approximated Heavside-function(1.45). Combined with eq (1.44), this gives us

$$h(\phi) = \begin{cases} 50, \text{ if } \phi < -\tau, \\ 100, \text{ if } \phi > \tau, \\ 50 + 25\left[1 + \dfrac{\phi}{\tau} + \dfrac{1}{\pi}\sin\left(\dfrac{\pi\phi}{\tau}\right)\right], \text{ if } |\phi| \leq \tau. \end{cases} \tag{1.61}$$

To make this more stringent we will introduce an operator describing this mapping. Let $S : \mathbb{R}^4 \longmapsto H^1(H)$ be defined by

$$S(x_0, y_0, z_0, s) = h(x; x_0, y_0, z_0, s). \tag{1.62}$$

What we see, is that we take a element from $\mathbb{R}^4$ and send it to the operator S, and get out a $H^1(H)$-function, as the one defined in (1.61). Now, we observe that this is a non-linear operator.

When we now describe the full forward problem, it can be defined by the operator

$$F = TL^{-1}QS : \mathbb{R}^4 \longmapsto L^2(\partial B), \tag{1.63}$$

where the operators on the right-hand side is from (1.37), (1.49), (1.50) and (1.62). This will then be a non-linear operator because of the operator S. Hence, we might hope to gain more stability by approximating the ischemic region as a ball, but we do lose linearity. Nevertheless, all these topics will be discussed either theoretically or numerically in this thesis.

2 Continuity properties of the system

This section will be spent looking at the mapping from input parameters to the electrocardiogram, and decide whether this mapping is continuous. If so, Weierstrass' theorem will imply that on a compact domain the operator will have a minimum. Hence, if this forward mapping is continuous, we know that there exists an ischemic region in the heart providing a minimum for the cost-functional, J(1.40).

2.1 Continuity of the forward operator

In the introduction, some of the operators were just quickly defined, so we will look more closely at them now, and then be able to analyze the continuity properties of each of the operators. But first, we will just give a short written review of the problem we face.

Initially, we assumed a ball-shaped geometry for the ischemic region. We need four parameters to represent this shape(three for the center and one for the radius). After mapping these parameters to a $H^1(H)$-function(1.61), we are able to solve the PDE (1.22). The solution to this PDE is a $H^1(B)$-function describing the extracellular potential throughout the body. By the use of the trace theorem, we can also map this to a L^2-function defined on the boundary of the body. This, however, is a theoretical function, without much practical use, since we need point-values at the electrodes. Therefore, we must use some kind of average of the function around each electrode, to take care of the fact that a L^2-function is undefined for a set of measure zero.

Now, we would like to show that all these operations are continuous, but let us first state the definition of a continuous operator, as well as of a Lipschitz continuous operator:

Definition - Continuity Let X and Y be normed spaces. An operator $f : X \longrightarrow Y$ is *continuous* at $x_0 \in X$ if for every $\epsilon > 0$, there exists a $\delta > 0$ such that

$$\|f(x) - f(x_0)\|_Y < \epsilon$$

whenever

$$\|x - x_0\|_X < \delta.$$

Definition - Lipschitz continuity An operator $f : X \longrightarrow Y$ is *Lipschitz continuous* if there exists a $M \in \mathbb{R}$ such that

$$\|f(x) - f(x_0)\|_Y < M\|x - x_0\|_X, \quad \forall x, x_0 \in X.$$

We did discuss the trace operator T(1.37) in the section about existence and uniqueness, and we did introduce the two operators L and Q associated with the PDE in eq (1.49) and (1.50). Finally, in the last section of the previous chapter, we did introduce the mapping S from the ischemic domain to the shift in the transmembrane potential(1.62). Of these operators, we know that T, L^{-1} and Q are linear, so if these turns out to be continuous, it follows automatically that they are Lipschitz continuous (Proof 1 - Appendix A). This is a much stronger type of continuity, so we'll as far as possible try to show Lipschitz continuity of the different operators. The reason for doing so, is due to our goal of increasing the stability. Lipschitz continuity implies a globally stability in our forward operator, and however not certain, but it might indicate a stronger stability of the inverse operator, if such is present.

If now the operator S is Lipschitz continuous as well, we know that F also will be a Lipschitz continuous operator, since the composition of (Lipschitz) continuous operators are (Lipschitz) continuous (Proof 2 - Appendix A). But before using the definitions of continuity and these two small proofs to show continuity of the forward operator, we need one more theorem first.

Bounded inverse theorem Let X and Y be Banach spaces. Let $f : X \longmapsto Y$ be a bounded, linear and bijective operator. Then it follows that f^{-1} is bounded as well.

A proof of this theorem can be found in a standard textbook in functional analysis (see e.g [25]). Now however, we can move on to the continuity theorem. Just note that we now use the standard symbol for $H^1(B)$ and not the subspace X as we introduced earlier(1.21). This is done to make the proof easier to follow. Even though S, Q, L^{-1} and T operates on subspaces of the commonly known spaces below, we are about to prove several inequalities, so it does not make any practical differences, since the norms of the subspaces are inherited from the spaces themselves. The theorem is stated as:

THEOREM 1 - Continuity of forward operator Given the partial differential equation

$$Lr = QS\{x_0, y_0, z_0, s\}, \tag{2.1}$$

from (1.22, 1.27 and 1.53), along with the mapping from (1.62). Then the mapping F (1.63), denoted by the composition of operators given as

$$\mathbb{R}^4 \xrightarrow{S} H^1(H) \xrightarrow{Q} H^1(B)^* \xrightarrow{L^{-1}} (H^1(B)) \xrightarrow{T} L^2(\partial B),$$

is Lipschitz continuous.

Proof: The trace theorem has already shown that T is continuous, so it remains to see if the remaining operators are continuous.

Step 1 (The L^{-1}-operator): To consider L^{-1}, we remember the bilinear form

$$\hat{L}(r,\psi) = \int_B \nabla\psi \cdot (M\nabla r)dx,\ \ r,\psi \in H^1(B). \tag{2.2}$$

From this, the previously introduced $L:\ X \to X^*$ was defined as

$$\langle Lr,\psi\rangle\ = \hat{L}(r,\psi), \tag{2.3}$$

where X is from eq (1.21). We have to use this subspace right now, and not $H^1(B)$, since this operator is not a bijection from $H^1(B)$ to $H^1(B)^*$. Nevertheless, the goal is to prove that L is a continuous and bijective operator, for if so, it follows from the bounded inverse theorem that the inverse exists and that this is bounded as well. With use of Riesz representation theorem, we have already shown that L is an isometric isomorphism. So, it follows that L is continuous, and hence that L^{-1} is bounded, and equivalently continuous.

Step 2 (The Q-operator): Similarly, the operator $Q:\ H^1(H) \to (H^1(B))^*$ was defined by

$$\langle Qh,\psi\rangle = -\int_H \nabla\psi \cdot (M_i\nabla h)\ dx,\ \ \ h,\psi \in H^1(B), \tag{2.4}$$

so, by using the definition of the norm on the dual space, we get

$$\begin{aligned}\|Qh\|_{(H^1(B))^*} &= \sup_{\|\psi\|_{H^1(B)}\leq\ 1} \left|\int_H \nabla\psi \cdot (M_i\nabla h)\right| dx \\ &\leq \sup_{\|\psi\|_{H^1(B)}\leq\ 1} \int_H |\nabla\psi \cdot (M_i\nabla h)| dx \\ &\leq C \sup_{\|\psi\|_{H^1(B)}\leq 1} \|\psi\|_{H^1(B)}\|h\|_{H^1(B)} \leq C\|h\|_{H^1(B)}. \end{aligned} \tag{2.5}$$

Hence, this mapping is also continuous. It now remains to show that the S-operator(1.62) is Lipschitz continuous. However, we deduced in the end of the last chapter that S was non-linear, and hence the equivalence between boundedness and continuity is no longer present. So, it must be shown explicitly that a small change in the ischemic region will provide a small change in the H^1-function generated by S.

Step 3 (Show that $h \in H^1(H)$): The operator S is a mapping to $H^1(H)$. This means that a small change in the ischemic region must give a corresponding small change in both the function itself as well as its weak derivative under the L^2-norm. But before calculating these norms, we must prove that that h (1.61) actually is an element in $H^1(H)$. Writing out $h(\phi(x;\tilde{x}))$, where $\tilde{x} = (x_0, y_0, z_0, s)$, it reads

$$h(\phi(x;\tilde{x})) = \begin{cases} 50 & \text{if } \phi < -\tau, \\ 100 & \text{if } \phi > \tau, \\ 50 + 25\left[1 + \frac{\phi}{\tau} + \frac{1}{\pi}\sin\left(\frac{\pi\phi}{\tau}\right)\right] & \text{if } |\phi| \leq \tau. \end{cases}$$

Note that, since ϕ (1.46) is a smooth function, we can see from the expression above that $h(\phi)$ also is a continuous function, i.e, $h(\phi) \in C(H)$. Further, the derivative is

$$\nabla h(\phi(x;\hat{x})) = \begin{cases} 0 & \text{if } |\phi| > \tau, \\ 50\left[\frac{1}{\tau} + \frac{1}{\tau}\cos\left(\frac{\pi\phi}{\tau}\right)\right]\nabla\phi(x;\tilde{x}) & \text{if } |\phi| \leq \tau. \end{cases}$$

which is also a continuous function since in fact $\phi \in C^\infty(H)$ (it suffices that $\phi \in C^1(H)$). Hence $h(\phi)$ is a function in $C^1(H)$, and then also in $H^1(H)$ since the domain in bounded.

Step 4 (The S-operator): If we can show that the mappings $S_1 : \mathbb{R}^4 \longmapsto H^1(H)$ defined by

$$S_1(\tilde{x}) = \phi(x;\tilde{x}), \tag{2.6}$$

and $S_2 : H^1(H) \longmapsto H^1(H)$ defined by

$$S_2(\phi) = h(\phi), \tag{2.7}$$

are Lipschitz continuous, it follows that S is Lipschitz continuous, since $S = S_2 \circ S_1$. Here ϕ is the function from eq (1.46) and h is from eq (1.61).

When considering the mapping S_1, we start by looking at the H^1-norm. That is, we must measure the distance between both the functions themselves, as well as their derivative in the L^2-sense. We first note, however, that we need to label several variables now, so in the next few calculations, we will use boldface for the vector-valued variables, and normal letters for variables and parameters in $\mathbb{R}$. This is not done elsewhere in the text, due to the fact that it should be clear from the setting which is meant. We now start to consider the mapping by looking at the distance between the two functions in L^2-norm:

$$\begin{aligned}\|\phi(\mathbf{x};\tilde{\mathbf{x}})-\phi(\mathbf{x};\tilde{\mathbf{x}}_0)\|^2_{L^2(H)} &= \int_H |(x-x_0)^2+(y-y_0)^2+(z-z_0)^2-s^2\\ &-((x-\tilde{x}_0)^2-(y-\tilde{y}_0)^2-(z-\tilde{z}_0)^2-\tilde{s}^2)|^2 d\mathbf{x}\\ &= \int_H |[x_0^2-\tilde{x}_0^2+y_0^2-\tilde{y}_0^2+z_0^2-\tilde{z}_0^2+(\tilde{s}^2-s^2)]\\ &+2x(\tilde{x}_0-x_0)+2y(\tilde{y}_0-y_0)+2z(\tilde{z}_0-z_0)|^2 d\mathbf{x}\\ &\overset{Minkowski's}{\leq} (\|x_0^2-\tilde{x}_0^2+y_0^2-\tilde{y}_0^2+z_0^2-\tilde{z}_0^2+(\tilde{s}^2-s^2)\|_{L^2(H)}\\ &\quad+\|2x(\tilde{x}_0-x_0)+2y(\tilde{y}_0-y_0)+2z(\tilde{z}_0-z_0)\|_{L^2(H)})^2. \end{aligned} \tag{2.8}$$

Now, we must evaluate both of these terms to find a bound. Starting with the first, we can rewrite this as

$$\begin{aligned}&\|x_0^2-\tilde{x}_0^2+y_0^2-\tilde{y}_0^2+z_0^2-\tilde{z}_0^2+(\tilde{s}^2-s^2)\|_{L^2(H)}\\ &=\|(x_0-\tilde{x}_0)(x_0+\tilde{x}_0)+(y_0-\tilde{y}_0)(y_0+\tilde{y}_0)+(z_0-\tilde{z}_0)(z_0+\tilde{z}_0)+(\tilde{s}-s)(\tilde{s}+s)\|_{L^2(H)}\\ &\overset{Minkowski's}{\leq} |x_0+\tilde{x}_0|\|x-\tilde{x}_0\|_{L^2(H)}+|y_0+\tilde{y}_0|\|y-\tilde{y}_0\|_{L^2(H)}\\ &\quad+|z_0+\tilde{z}_0|\|z-\tilde{z}_0\|_{L^2(H)}+|s+\tilde{s}|\|\tilde{s}-s\|_{L^2(H)}\leq C\|\tilde{\mathbf{x}}-\tilde{\mathbf{x}}_0\|_{\mathbb{R}^4}. \end{aligned} \tag{2.9}$$

Note that since every parameter above is constant with respect to the Lebesgue measure, it is easy to pull expressions out of the norm. When moving on the second, we remark that the variables are bounded, since we are inside the heart. Therefore, we get

$$\begin{aligned}&\|2x(\tilde{x}_0-x_0)+2y(\tilde{y}_0-y_0)+2z(\tilde{z}_0-z_0)\|_{L^2(H)}\\ &\qquad\leq 2M\|(\tilde{x}_0-x_0)\|_{L^2(H)}+2M\|(\tilde{y}_0-y_0)\|_{L^2(H)}\\ &\qquad\quad+2M\|(\tilde{z}_0-z_0)\|_{L^2(H)}\leq C\|\tilde{\mathbf{x}}-\tilde{\mathbf{x}}_0\|_{\mathbb{R}^4}. \end{aligned} \tag{2.10}$$

Hence, we have a bound for the entire expression, so S_1 is a Lipschitz continuous mapping from $\mathbb{R}^4$ to L^2, but in addition, this must also hold for the derivative, which reads

$$\begin{aligned}&\|\nabla\phi(\mathbf{x};\tilde{\mathbf{x}})-\nabla\phi(\mathbf{x};\tilde{\mathbf{x}}_0)\|^2_{L^2(H)}\\ &=\int_H |2(x-x_0)-2(x-\tilde{x}_0)+2(y-y_0)-2(y-\tilde{y}_0)+2(z-z_0)-2(z-\tilde{z}_0)|^2 d\mathbf{x}\\ &\quad=\int_H |2(x_0-\tilde{x}_0)+2(y_0-\tilde{y}_0)+2(z_0-\tilde{z}_0)|^2 d\mathbf{x}\leq C\|\tilde{\mathbf{x}}-\tilde{\mathbf{x}}_0\|^2_{\mathbb{R}^4}. \end{aligned} \tag{2.11}$$

Thus, S_1 is a Lipschitz continuous operator from $\mathbb{R}^4$ to $H^1(H)$. Now, we will consider the mapping S_2. But note that our choice of $\phi \in C^1(H)$ was very specific. Thus, we are really limited in our choice of function to be used in the Heavside approximation(1.45). If we want to approximate the ischemic region as a square or a rectangle for instance, we need some other function to describe when we are inside and outside the ischemic region. In fact, we can actually take this into account now. We have already proved that the mapping $\tilde{x} \longmapsto \phi(x;\tilde{x})$ is Lipschitz continuous. Therefore, we can now neglect the shape of this function, and instead turn the attention to any function in the space $W^{1,\infty}(H) = \{u \in L^\infty(H) : \nabla u \in L^\infty(H)\}$. Clearly, the function ϕ we already mentioned (1.46), is in this space. Hence, if we can prove that the mapping $\eta \longmapsto h(\eta)$ is Lipschitz continuous for any $\eta \in W^{1,\infty}(H)$, the theorem will follow. Then it will merely be a question about showing that a mapping $\tilde{x} \longmapsto \eta(x;\tilde{x})$ is Lipschitz continuous to obtain a Lipschitz continuous forward operator when working with different shapes for the ischemic region, represented by the η-function.

This expansion, however, requires us to show that $h(\eta) \in H^1(H)$ when $\eta \in W^{1,\infty}(H)$, which is true due to

$$\begin{aligned}
&\|h(\eta(x;\tilde{x}))\|^2_{L^2(B)} \\
&= \int_{\eta<-\tau} 50^2 dx + \int_{\eta>\tau} 100^2 dx + \int_{|\eta|\le\tau} \left|50 + 25\left[1 + \frac{\eta}{\tau} + \frac{1}{\pi}\sin\left(\frac{\pi\eta}{\tau}\right)\right]\right|^2 dx \\
&\le 100^2 \int_H dx < \infty, \quad (2.12)
\end{aligned}$$

for the function itself, and for the derivative we get the estimate

$$\begin{aligned}
&\|\nabla h(\eta(x;\tilde{x}))\|^2_{L^2(B)} = \int_{|\eta|\le\tau} \left|50\left[\frac{1}{\tau} + \frac{1}{\tau}\cos\left(\frac{\pi\eta}{\tau}\right)\right]\nabla\eta\right|^2 dx \\
&\le \left(\frac{100}{\tau}\right)^2 \int_{|\eta|\le\tau} |\nabla\eta|^2 dx \le \left(\frac{100}{\tau}\right)^2 \left(\sup_{x\in H}|\nabla\eta|\right)^2 \int_{|\eta|\le\tau} dx < \infty. \quad (2.13)
\end{aligned}$$

Hence, we can return to the mapping S_2, which is quite technical, so we will start by writing out

$$h(\eta) - h(\eta_0) = \begin{cases}
0 & \text{if } \eta, \eta_0 < -\tau, \\
-25[1 + \frac{\eta_0}{\tau} + \frac{1}{\pi}\sin(\frac{\pi\eta_0}{\tau})] & \text{if } \eta < -\tau, |\eta_0| \le \tau, \\
50 & \text{if } \eta < -\tau, \eta_0 > \tau, \\
25[1 + \frac{\eta}{\tau} + \frac{1}{\pi}\sin(\frac{\pi\eta}{\tau})] & \text{if } |\eta| \le \tau, \eta_0 < -\tau, \\
25[\frac{\eta-\eta_0}{\tau} + \frac{1}{\pi}(\sin(\frac{\pi\eta}{\tau}) - \sin(\frac{\pi\eta_0}{\tau}))] & \text{if } |\eta|, |\eta_0| \le \tau, \\
25[1 + \frac{\eta}{\tau} + \frac{1}{\pi}\sin(\frac{\pi\eta}{\tau})] - 50 & \text{if } |\eta| \le \tau, \eta_0 > \tau, \\
50 & \text{if } \eta > \tau, \eta_0 < -\tau, \\
50 - 25[1 + \frac{\eta_0}{\tau} + \frac{1}{\pi}\sin(\frac{\pi\eta_0}{\tau})] & \text{if } \eta > \tau, |\eta_0| \le \tau, \\
0 & \text{if } \eta, \eta_0 > \tau.
\end{cases}$$

Now, what must be proven is Lipschitz continuity of S_2 from $W^{1,\infty}$ to H^1. To do so, we will first consider each of the nine parts of the above expression, and try do find a bound on them in L^2-sense. Also, we will denote each of these domains from D_1 to D_9, starting from the top, to make the integral symbols cleaner. The first and the last domain of the integral, however, will not contribute to the integral. So, we start of with the second part, but first note the similarity between the second and forth expression. In fact, these will have the same bound in L^2-sense, so if suffices to consider one of them. So, by looking at the second part, we get

$$\begin{aligned}\|h(\eta)-h(\eta_0)\|^2_{L^2(D_2)} &= \int_{D_2}\left|-25\left[1+\frac{\eta_0}{\tau}+\frac{1}{\pi}\sin\left(\frac{\pi\eta_0}{\tau}\right)\right]\right|^2 dx\\ &= 25^2\int_{D_2}\left|1+\frac{\eta_0}{\tau}+\frac{1}{\pi}\sin\left(\frac{\pi\eta_0}{\tau}\right)\right|^2 dx\\ &\overset{Minkowski's}{\leq} 25^2\left(\left\|1+\frac{\eta_0}{\tau}\right\|_{L^2(D_2)}+\left\|\frac{1}{\pi}\sin\left(\frac{\pi\eta_0}{\tau}\right)\right\|_{L^2(D_2)}\right)^2. \end{aligned} \tag{2.14}$$

These two new terms much be considered, and starting out with the first, we get

$$\begin{aligned}\left\|\frac{\eta_0}{\tau}+1\right\|^2_{L^2(D_2)} &= \int_{D_2}\left|\frac{\eta_0}{\tau}+1\right|^2 dx\\ &= \int_{D_2}\left|\frac{\eta_0}{\tau}+\frac{\tau}{\tau}\right|^2 dx \leq \int_{D_2}\left|\frac{\eta_0}{\tau}-\frac{\eta}{\tau}\right|^2 dx \leq C\|\eta-\eta_0\|^2_{L^2(H)}, \end{aligned} \tag{2.15}$$

due to the fact that in this domain, $\eta < -\tau$, which we used to obtain the inequality. Furthermore, the other term can be bounded as

$$\begin{aligned}\left\|\frac{1}{\pi}\sin\left(\frac{\pi\eta_0}{\tau}\right)\right\|^2_{L^2(D_2)} &= \int_{D_2}\left|\frac{1}{\pi}\sin\left(\frac{\pi\eta_0}{\tau}\right)\right|^2 dx\\ &= \int_{D_2}\left|\frac{1}{\pi}\sin\left(\frac{\pi\eta_0}{\tau}+\frac{\pi\tau}{\tau}\right)\right|^2 dx \leq \int_{D_2}\left|\frac{1}{\pi}\left(\frac{\pi\eta_0}{\tau}+\frac{\pi\tau}{\tau}\right)\right|^2 dx\\ &\leq \int_{D_2}\left|\frac{\eta_0-\eta}{\tau}\right|^2 dx \leq C\|\eta-\eta_0\|^2_{L^2(H)}, \end{aligned} \tag{2.16}$$

by the same argument as above. Hence, this first expression holds. Next, we consider the third and seventh part, which is given by

$$\int_{D_3\cup D_7} 50^2 dx \leq \frac{50^2}{4\tau^2}\int_{D_3\cup D_7}|\eta-\eta_0|^2 dx \leq \frac{50^2}{4\tau^2}\|\eta-\eta_0\|^2_{L^2(H)}, \tag{2.17}$$

since the distance $|\eta-\eta_0|$ is larger than 2τ in this part of the integral.

Hence, six of the nine parts are under control. Furthermore, we can observe that the sixth and the eight part of the mapping, is also similar in the sense of the L^2-norm, so we can once more consider only one of them.

$$\int_{D_6} \left| 25 \left[-1 + \frac{\eta}{\tau} + \frac{1}{\pi} \sin\left(\frac{\pi\eta}{\tau}\right) \right] \right|^2 dx$$
$$= 25^2 \int_{D_6} \left| -1 + \frac{\eta}{\tau} + \frac{1}{\pi} \sin\left(\frac{\pi\eta}{\tau}\right) \right|^2 dx$$
$$\overset{Minkowski's}{\leq} 25^2 \left(\left\| -1 + \frac{\eta}{\tau} \right\|_{L^2(D_6)} + \left\| \frac{1}{\pi} \sin\left(\frac{\pi\eta}{\tau}\right) \right\|_{L^2(D_6)} \right)^2. \quad (2.18)$$

We can observe that the second term in this last expression is equal to the second term in the inequality in expression (2.14), and thus if suffices to evaluate the first term. However, we can apply the argument that $|-1+\frac{\eta}{\tau}| \leq |\frac{\eta-\eta_0}{\tau}|$ in this domain as well, and the same bound as in (2.15) holds. Hence, the only domain it remains to consider is the fifth, given by

$$\int_{D_5} \left| 25 \left[\frac{\eta-\eta_0}{\tau} + \frac{1}{\pi} \left(\sin\left(\frac{\pi\eta}{\tau}\right) - \sin\left(\frac{\pi\eta_0}{\tau}\right) \right) \right] \right|^2 dx$$
$$\overset{Minkowski's}{\leq} 25^2 \left(\frac{1}{\tau} \|\eta-\eta_0\|_{L^2(H)} + \frac{1}{\pi} \left\| \sin\left(\frac{\pi\eta}{\tau}\right) - \sin\left(\frac{\pi\eta_0}{\tau}\right) \right\|_{L^2(D_5)} \right)^2. \quad (2.19)$$

Now, let's consider the second part of this, since the first is already on the desired form. To do so, we will use the trigonometric relation $sin(A) - sin(B) = 2cos((A+B)/2)sin((A-B)/2)$, and hence, the expression becomes

$$\left\| \sin\left(\frac{\pi\eta}{\tau}\right) - \sin\left(\frac{\pi\eta_0}{\tau}\right) \right\|_{L^2(D_5)}$$
$$= \left\| 2\cos\left(\frac{\pi(\eta+\eta_0)}{2\tau}\right) \sin\left(\frac{\pi(\eta-\eta_0)}{2\tau}\right) \right\|_{L^2(D_5)}$$
$$\leq 2 \left\| \sin\left(\frac{\pi(\eta-\eta_0)}{2\tau}\right) \right\|_{L^2(D_5)} \leq 2 \left\| \left(\frac{\pi(\eta-\eta_0)}{2\tau}\right) \right\|_{L^2(D_5)}$$
$$\leq C\|\eta-\eta_0\|_{L^2(H)}. \quad (2.20)$$

Thus, we have shown that the mapping is Lipschitz continuous from $W^{1,\infty}(H)$ to $L^2(H)$. To prove further, that S_2 is a Lipschitz continuous mapping from $W^{1,\infty}(H)$ to $H^1(H)$, we must now consider the derivatives. So, first we will state the expression

$$\nabla(h(\eta) - h(\eta_0))$$
$$= \begin{cases} 0 & \text{if } |\eta|, |\eta_0| > \tau, \\ \frac{25}{\tau}[1+\cos(\frac{\pi\eta}{\tau})]\nabla\eta & \text{if } |\eta| \leq \tau, |\eta_0| > \tau, \\ \frac{25}{\tau}[1+\cos(\frac{\pi\eta_0}{\tau})]\nabla\eta_0 & \text{if } |\eta| > \tau, |\eta_0| \leq \tau, \\ \frac{25}{\tau}\left([1+\cos(\frac{\pi\eta}{\tau})]\nabla\eta - [1+\cos(\frac{\pi\eta_0}{\tau})]\nabla\eta_0\right) & \text{if } |\eta|, |\eta_0| \leq \tau. \end{cases}$$

Hence, there are four domains to consider, denoted from D_1 to D_4. The first domain, however, will clearly not contribute. So, we move on to the second, and also the third, since these will have an equal bound. Applying some trigonometric relations, we get the inequalities

$$\begin{aligned}
\|\nabla h(\eta) - \nabla h(\eta_0)\|^2_{L^2(D_2)} &= \int_{D_2} \left| \frac{25}{\tau} \left[1 + \cos\left(\frac{\pi\eta}{\tau}\right)\right] \nabla\eta \right|^2 dx \\
&= \left(\frac{25}{\tau}\right)^2 \int_{D_2} \left| \left(\cos\left(\frac{\pi\eta}{\tau}\right) - \cos\left(\frac{\pi\tau}{\tau}\right)\right) \nabla\eta\right|^2 dx \\
&= \left(\frac{25}{\tau}\right)^2 \int_{D_2} \left| 2\sin\left(\frac{\pi\eta + \pi\tau}{\tau}\right) \sin\left(\frac{\pi\eta - \pi\tau}{\tau}\right) \nabla\eta\right|^2 dx \\
&\leq \left(\frac{50}{\tau}\right)^2 \|\nabla\eta\|^2_{L^\infty} \int_{D_2\cap\{\eta_0>\tau\}} \left|\sin\left(\frac{\pi\eta - \pi\tau}{\tau}\right)\right|^2 dx \\
&+ \left(\frac{50}{\tau}\right)^2 \|\nabla\eta\|^2_{L^\infty} \int_{D_2\cap\{\eta_0<-\tau\}} \left|\sin\left(\frac{\pi\eta + \pi\tau}{\tau}\right)\right|^2 dx \\
&\leq \left(\frac{50}{\tau}\right)^2 \|\nabla\eta\|^2_{L^\infty} \int_{D_2\cap\{\eta_0>\tau\}} \left|\frac{\pi\eta - \pi\eta_0}{\tau}\right|^2 dx \\
&+ \left(\frac{50}{\tau}\right)^2 \|\nabla\eta\|^2_{L^\infty} \int_{D_2\cap\{\eta_0<-\tau\}} \left|\frac{\pi\eta - \pi\eta_0}{\tau}\right|^2 dx \leq C\|\eta - \eta_0\|^2_{L^2(H)}.
\end{aligned} \tag{2.21}$$

Note that we had to split the integral in two parts, and then use different sine-expression on each part, and bound the other simply by $|sin(x) \leq 1|$. The last part to consider now, is the expression in the fourth domain, given by

$$\begin{aligned}
&\|\nabla h(\eta) - \nabla h(\eta_0)\|_{L^2(D_4)} \\
&= \left\| \nabla\eta + \nabla\eta\cos\left(\frac{\pi\eta}{\tau}\right) - \nabla\eta_0 - \nabla\eta_0\cos\left(\frac{\pi\eta_0}{\tau}\right)\right\|_{L^2(D_4)} \\
&\leq \|\nabla\eta - \nabla\eta_0\|_{L^2(D_4)} + \left\|\nabla\eta\cos\left(\frac{\pi\eta}{\tau}\right) - \nabla\eta_0\cos\left(\frac{\pi\eta_0}{\tau}\right)\right\|_{L^2(D_4)} \\
&= \|\nabla\eta - \nabla\eta_0\|_{L^2(D_4)} + \left\|(\nabla\eta - \nabla\eta_0 + \nabla\eta_0)\cos\left(\frac{\pi\eta}{\tau}\right) - \nabla\eta_0\cos\left(\frac{\pi\eta_0}{\tau}\right)\right\|_{L^2(D_4)} \\
&\leq C|\eta - \eta_0\|_{H^1(D_4)} + \left\|\nabla\eta_0\left(\cos\left(\frac{\pi\eta}{\tau}\right) - \cos\left(\frac{\pi\eta_0}{\tau}\right)\right)\right\|_{L^2(D_4)} \\
&\leq C|\eta - \eta_0\|_{H^1(D_4)} + \|\nabla\eta_0\|_{L^\infty} \left\|\frac{\pi}{\tau}(\eta - \eta_0)\right\|_{L^2(D_4)} \leq C|\eta - \eta_0\|_{H^1(H)}.
\end{aligned} \tag{2.22}$$

Hence, the theorem follows.

Now, we have proved that the mapping F (1.63) is Lipschitz continuous. But before discussing this any further, we will just show a corollary to expand the class of level-set functions.

Corollary 1 For any $\eta(x; x_0, y_0, z_0, s) \in W^{1,\infty}(H)$ for which the mapping $(x_0, y_0, z_0, s) \longmapsto \eta(x; x_0, y_0, z_0, s)$ is Lipschitz continuous, then

$F = TL^{-1}Q\{h(\eta(x_0, y_0, z_0, s))\}$ is Lipschitz continuous.

Proof: This follows directly from the proof of Theorem 1.

As mention in the beginning of this section, the mapping to the boundary is actually an L^2-function, but in real life, we only have a finite set of electrodes. To get an evaluation at these point, we want to average the L^2-function around each of these, to get

$$\frac{1}{|\partial B(x_i, \epsilon)|} \int_{\partial B(x_i,\epsilon)} u(x)dS, \tag{2.23}$$

where $B(x_i, \epsilon)$ is a ball with center in x_i and radius of ϵ, for some predefined $\epsilon > 0$. Now, we want to show that this is also a continuous operation. Let $A : L^2(\partial B) \longmapsto \mathbb{R}^n$ be defined by

$$Au = \frac{1}{|\partial B(x_i, \epsilon)|} \int_{\partial B(x_i,\epsilon)} u(x)dS, \tag{2.24}$$

so by letting $u, v \in L^2(\partial B),\ \alpha, \beta \in \mathbb{R}$ we get

$$\begin{aligned} A(\alpha u + \beta v) &= \frac{1}{|\partial B(x_i, \epsilon)|} \int_{\partial B(x_i,\epsilon)} \alpha u(x) + \beta v(x)dS \\ &= \alpha \frac{1}{|\partial B(x_i, \epsilon)|} \int_{\partial B(x_i,\epsilon)} u(x)dS + \beta \frac{1}{|\partial B(x_i, \epsilon)|} \int_{\partial B(x_i,\epsilon)} v(x)dS \\ &= \alpha Au + \beta Av. \end{aligned} \tag{2.25}$$

Hence, this is linear, and by Hölder's inequality, we get

$$\begin{aligned} &\frac{1}{|\partial B(x_i, \epsilon)|} \int_{\partial B(x_i,\epsilon)} 1 * u(x)dS \\ &\quad \leq \frac{1}{|\partial B(x_i, \epsilon)|} \|1\|_{L^2(\partial B)} \frac{1}{|\partial B(x_i, \epsilon)|} \|u\|_{L^2(\partial B)} \leq C\|u\|_{L^2(\partial B)}. \end{aligned} \tag{2.26}$$

Hence, since this operator A is bounded and linear, we get that this mapping is Lipschitz continuous as well, and therefore all the piecewise mappings is continuous. From Appendix A, we then also have that the cost-functional J (1.40) is continuous. Thus, for a given BSPM(Body Surface Potential Mapping), there does in fact, from Weierstrass' theorem, exist a ischemic region providing a minimum for the cost-functional, provided that the set of ischemic parameters is chosen to be compact. However, we need to show if we can find the ischemic region when we have a recorded BSPM, and whether this ischemic region depends continuously on the BSPM.

2.2 How to obtain continuous inverse and continuous least-squares

When considering the forward operator, we looked at $F : \mathbb{R}^4 \longmapsto \mathbb{R}^n$, where n is the number of electrodes attached to the body. We found this operator to be continuous, and thus the cost-functional is continuous as well. Our main objective, however, is to use the BSPM to determine the localization and size of the ischemic region, in the sense of minimizing the cost-functional(1.40).

It will not automatically follow that this least-squares solution will exist for all BSPM assuming F (1.63) is invertible, but we claim for this to be a necessary requirement for such a minimum solution to exist. To show this, we assume $d \in R(F)$, where $R(F)$ denotes the image of the operator F. This implies the existence of x such that $F(x) = d$. In this case, we need to invert F to find x, which will be our solution to the minimization of the cost-functional (since J(x) = 0 in this case). Hence, to find back to the ischemic region assuming the BSPM is in the image of the forward operator, we need for F to be invertible. When the BSPM lies outside the image, we need more requirements to obtain a continuous least-squares solution, but this will be discussed later.

But in addition to F having an inverse, we want this to be continuous, since a small change in the BSPM should provide a small change in the ischemic region. So, assuming that the inverse exists, what can we say about the continuity property? Since we are in finite dimensions, it might be reasonable to assume this being the case regardless of domains, but the following 1D example shows us that this is not the case:

Example: Let $f : [0, 1) \cup [2, 3] \longmapsto [0, 2]$ be defined by

$$f(x) = \begin{cases} x & \text{in } [0,1) \\ x-1 & \text{in } [2,3]. \end{cases}$$

Then, clearly, f is continuous, one-to-one and onto. That is, continuous and bijective. Nevertheless, as shown in Figure 4, the inverse is discontinuous, which shows that a finite dimensional domain is not sufficient to obtain a continuous inverse. A natural question is what happens if you include the point $\{1\}$ in the domain, but then two elements in the domain maps to the same element in the range, and the function is no longer injective.

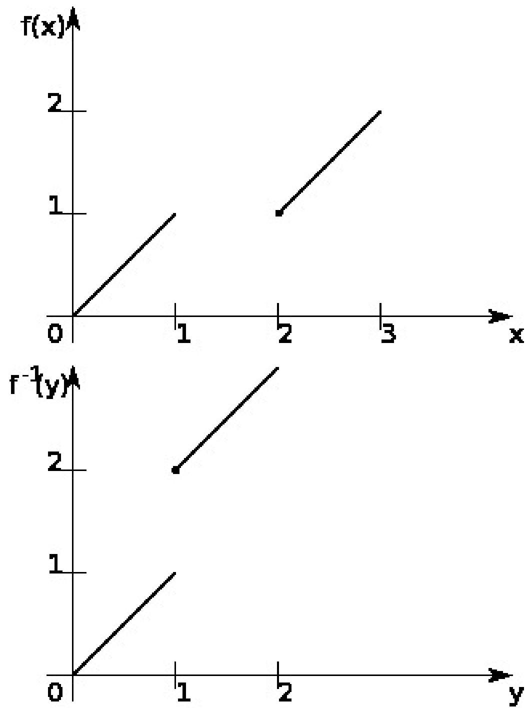

Figure 4: Discontinuous inverse

It might also be reasonable to believe it to be the fact that the domain is disconnected that gets us into trouble, but the function $f(x) = (\cos\ x, \sin\ x)$ from $[0, 2\pi)$ to the unit circle in $\mathbb{R}^2$ will also give us a discontinuous inverse. Hence, we must strengthen the requirements of the domain, and assume it to be compact. For a closed and bounded domain, i.e, a compact domain, where F is a bijection, we have a continuous inverse from a theorem in topology [5, 6], which says that:

Theorem 2 - Continuity of the inverse operator

Let X be compact and Y be a normed space. Further, assume $T : X \longmapsto Y$ is continuous and bijective. Then the mapping T is a homeomorphism.

The proof can be found in both these books, but we choose to add a proof here, to highlight some concepts in topology not discussed anywhere else in this thesis.

Proof: Let $B \subset X$ be open. Then $X \setminus B$ is closed, and hence compact. Further, since T is continuous, a mapping from a compact set gives a compact image, thus $T(X \setminus B)$ is compact in Y, and hence closed. Further, we get that $T(X \setminus B) = T(X) \setminus T(B)$ since T is a bijection. Hence, $T(B)$ is open. From this, we conclude that every open $B \subset X$ for the mapping $T^{-1} : Y \longmapsto X$ the preimage $T(B)$ is open, and hence is T^{-1} continuous.

Here we used a more general definition on continuity. In a general topology, we do define continuity by open preimages. That is, for a mapping $f : X \longmapsto Y$, then f is continuous if for every open $M \subset Y$, then the preimage $f^{-1}[M] = \{x \in X : f(x) \in M\}$ is open. So, when we use a norm as topology, this relates to "open balls" around a point, for which the points mapped through the function must lie inside another ball in the image.

Also, we claimed that a closed subset of a compact space is compact. This is easy to prove by the fact that every sequence in the subset is also a sequence in the space itself, and thus has a convergent subsequence. But, since the subset is closed, this limit point must lie inside the subset, and thus every sequence in the subset has a convergent subsequence, and it follows that the subset is compact as well.

We have shown that if we choose a small compact domain inside the heart for which F is a bijection, we will have a continuous inverse. It is not likely, however, that the BSPM will be in the range of F. Then, will the least-squares solution be unique? We know that the range, $R(F)$, of F will be closed, since it is compact. If we in addition, could assume that $R(F)$ is convex, we will have a unique least-squares solution, from a result in functional analysis [7, 8]:

Lemma - Unique least-squares solution

Given a non-empty, closed, convex subset D of a Hilbert space H, there exists a unique point $p \in D$ closest to a given point $x \in H$.

We do not, however, have any guarantee that the range $R(F)$ of F is convex. We ended Chapter 1 with a discussion around the fact that F (1.63) is non-linear. If it had been linear, such a guarantee would be available, as proven in the following lemma:

Lemma - Linearity preserves convexity Assume $T : X \longmapsto Y$ is linear, and X is convex. Then the range $R(T)$ of T is convex.

Proof: Let $x, y \in X$, $t \in [0, 1]$. Then

$$tT(x) + (1-t)T(y) = T(tx) + T((1-t)y) = T(tx + (1-t)y) \in R(T)$$

because $tx + (1-t)y \in X$ since X is convex. Hence $R(T)$ is convex.

Now, since F is non-linear, we will probably not have convexity, and therefore we will not necessarily obtain a unique point in the image $F(D)$ of F closest to an arbitrary BSPM in $\mathbb{R}^n$. Much work has been done trying to determine how far outside the image you can go and still obtain a continuous least-squares solution (see [14]). Unfortunately, although the theory is solid, it is really hard to use for problems like (1.41) - (1.42). Therefore, this will not be attempted, so we will instead speak more general about the demands for obtaining a continuous least-squares solution, and then afterwards present a drawing trying to visualize the point about how far outside the image you still can guarantee a continuous least-squares solution.

We now introduce some operators just for this brief section: Let $\mathcal{D} \subset \mathbb{R}^m$ be convex and compact. Further, let K be a continuous, linear and injective operator from $\mathcal{D}$ to $\mathbb{R}^n$. From the lemma above, we know that the image $K(\mathcal{D})$ is convex since K is linear. In addition, let $x \in \mathbb{R}^n$ be arbitrary. From the lemma about unique least-squares solution and the fact that $K(\mathcal{D})$ is closed and convex, we know that there will exists a unique point $y \in K(\mathcal{D})$ which is closest in norm to $x \in \mathbb{R}^n$.

Define the operator $U : \mathbb{R}^n \longmapsto K(\mathcal{D})$ by

$$Ux = y. \tag{2.27}$$

In other words, we define the operator U to be the operator which takes an arbitrary element in $\mathbb{R}^n$ and map it to the closest element in the image $K(\mathcal{D})$ of K. Thus, when we define the least-squares solution as

$$\min_{z \in \mathcal{D}} \|K(z) - x\|_{\mathbb{R}^m},$$

we will get the equality

$$\arg\min \|K(z) - x\|_{\mathbb{R}^m} = K^{-1}Ux,$$

since the right-hand side sends the element x to the closest solution in the image $K(\mathcal{D})$ of K, and then we use the inverse (which can be done since K is a bijection between $\mathcal{D}$ and $K(\mathcal{D})$) to retrieve the element in $\mathcal{D}$ corresponding to the element in the image. This operation is illustrated in Figure 5.

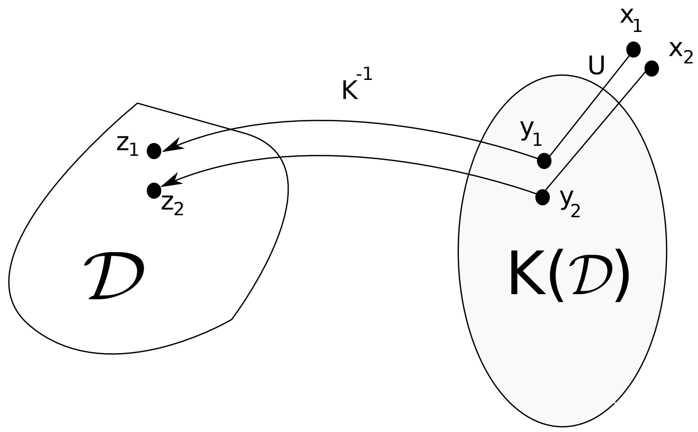

Figure 5: The least-squares solution of two different points. The first operator, U, takes two points in $\mathbb{R}^n$ and maps them to the image $K(\mathcal{D})$ of K. Then, we use the inverse of K to obtain the least-squares solution in $\mathcal{D}$. We have shown that under given assumptions, this operation is continuous, which we try to illustrate here (by letting the solutions lie close to each other for two points close in $\mathbb{R}^n$.

Now, we make use of a lemma in functional analysis (rewritten to fit our operators above), which states that the operator U we defined is continuous[7]:

Lemma - Continuity of minimizer Assume that the image $K(\mathcal{D})$ of K to be a compact subset of $\mathbb{R}^n$, and for every point $x \in \mathbb{R}^n$, there exists a unique closest point $y = Ux \in K(\mathcal{D})$. Then U is a continuous operator.

By assumption, this holds for (2.27). Therefore, we have that $K^{-1}U$ is a continuous operator, and thus we have a continuous least-squares solution.

To sum this up, we needed $\mathcal{D} \subset \mathbb{R}^m$ to be convex and compact. Hence, when we go back to our specific problem, we can just choose parameterization values from such a convex and compact subset $D \subset \mathbb{R}^4$. However, we had to assume the operator K to be continuous, injective and linear to obtain a closed and compact image, which in turn guaranteed a continuous least-squares solution. Again, referring to our specific problem, the operator F (1.63) is only certain to satisfy the first of these three requirements, and although it might satisfy the second (which will be discussed in Chapter

3), we have already shown that it do not satisfy the linearity requirement. Hence, we fail to obtain a certain stability outside the image $F(D)$ of the forward operator F. It does not, however, mean that such a stability can not be obtained close to the image of the forward operator. How far away from the image we can go, depend on how non-convex it is. This is being visualized in Figure 6.

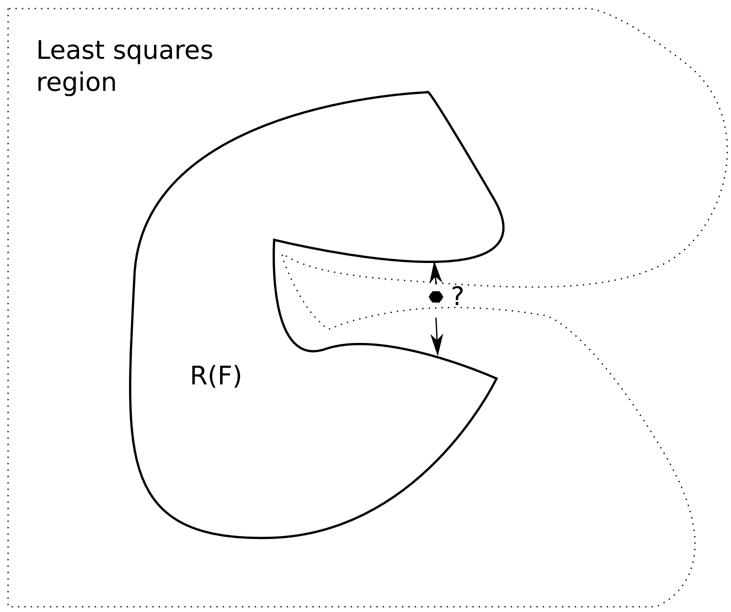

Figure 6: The area inside the solid drawing is the image of the forward operator, which is non-convex. The dotted drawing is trying to illustrate the area where we will have a continuous least-squares solution. The small black circle is trying to illustrate the point about discontinuity.

3 Uniqueness of ischemic region

As described in the previous section, we need a linear operator to guarantee a convex image. Unfortunately, we already know that this is not the case with the parameterization we made(1.46 and 1.61). On the other hand, we know that F is continuous (Theorem 1 - Chapter 2), and assuming that the forward operator F is a bijection, we will have a continuous inverse as long as we choose our ischemic parameters from a compact domain (Theorem 2 - Chapter 2).

But, although we do not have a convex set, we do not know *how* non-convex it is, in the sense that we might still obtain a continuous least-squares solution when we are close enough to the image of the forward operator, as illustrated in Figure 6.

However, we have yet to answer if we in fact have a one-to-one forward operator. That is, if two different ischemic regions always will produce two different BSPMs. To answer this, we will first consider the mapping $S : D \subset \mathbb{R}^4 \longmapsto H^1(H)$ (1.62), and then the mapping $TL^{-1}Q : H^1(H) \longmapsto L^2(\partial B)$, and raise the question if both of these are one-to-one. Remember that the composition of these operators in total makes up the forward operator. D was the subset of $\mathbb{R}^4$ consisting of the ischemic parameters.

3.1 Injectiveness of parameterization operator

We want to consider the uniqueness by first looking at the mapping $S : D \longmapsto H^1(H)$. Let $x_1, x_2 \in D, x_1 \neq x_2$ be arbitrary. We denote

$$S(x_1) = h(\phi(x; x_1)) = h_1 \tag{3.1}$$
$$S(x_2) = h(\phi(x; x_2)) = h_2. \tag{3.2}$$

Then, if we can show that

$$\int_H |h_1 - h_2|^2 dx \geq \Theta > 0, \tag{3.3}$$

it follows that $h_1 \neq h_2$. Hence, for any two arbitrary $x_1, x_2 \in D, x_1 \neq x_2 \Rightarrow S(x_1) \neq S(x_2)$. Then S is injective by definition.

In the previous chapter we thought of S as the composition of the mappings $\tilde{x} \longmapsto \phi(x; \tilde{x})$ and $\phi \longmapsto h(\phi)$. Hence, we can again make use of this by considering the mappings separately. First, however, let us write the expression for $h_2 - h_1$:

$$h_2 - h_1 = \begin{cases} 0 & \text{if } \phi_2, \phi_1 < -\tau, \\ -25[1 + \frac{\phi_1}{\tau} + \frac{1}{\pi}\sin(\frac{\pi\phi_1}{\tau})] & \text{if } \phi_2 < -\tau, |\phi_1| \leq \tau, \\ 50 & \text{if } \phi_2 < -\tau, \phi_1 > \tau, \\ 25[1 + \frac{\phi_2}{\tau} + \frac{1}{\pi}\sin(\frac{\pi\phi_2}{\tau})] & \text{if } |\phi_2| \leq \tau, \phi_1 < -\tau, \\ 25[\frac{\phi_2 - \phi_1}{\tau} + \frac{1}{\pi}(\sin(\frac{\pi\phi_2}{\tau}) - \sin(\frac{\pi\phi_1}{\tau}))] & \text{if } |\phi_2|, |\phi_1| \leq \tau, \\ 25[1 + \frac{\phi_2}{\tau} + \frac{1}{\pi}\sin(\frac{\pi\phi_2}{\tau})] - 50 & \text{if } |\phi_2| \leq \tau, \phi_1 > \tau, \\ 50 & \text{if } \phi_2 > \tau, \phi_1 < -\tau, \\ 50 - 25[1 + \frac{\phi_1}{\tau} + \frac{1}{\pi}\sin(\frac{\pi\phi_1}{\tau})] & \text{if } \phi_2 > \tau, |\phi_1| \leq \tau, \\ 0 & \text{if } \phi_2, \phi_1 > \tau. \end{cases}$$

Starting with the mapping $\tilde{\mathbf{x}} \longmapsto \phi(\mathbf{x}; \tilde{\mathbf{x}})$ from $\mathbb{R}^4$ to $H^1(H)$, we first hold the radius fixed, and only change one of the spherical parameters, say $\tilde{x}$, such that $\tilde{x} - \tilde{x}_0 = \epsilon_1$. Then we obtain

$$\int_H |\phi(\mathbf{x}; \tilde{\mathbf{x}}_2) - \phi(\mathbf{x}; \tilde{\mathbf{x}}_1)|^2 d\mathbf{x} = \int_H |(x - \tilde{x}_2)^2 - (x - \tilde{x}_1)^2|^2 \, d\mathbf{x}$$
$$= \int_H |(\tilde{x}_2 - \tilde{x}_1)(\tilde{x}_2 + \tilde{x}_1) + 2x(\tilde{x}_1 - \tilde{x}_2)|^2 d\mathbf{x} = \epsilon_1^2 \int_H |(\tilde{x}_2 + \tilde{x}_1) + 2x|^2 d\mathbf{x} = \epsilon_2^2 > 0. \quad (3.4)$$

Similarly, when we hold the center fixed, and instead change the radius, we obtain

$$\int_H |\phi(\mathbf{x}; \tilde{\mathbf{x}}_2) - \phi(\mathbf{x}; \tilde{\mathbf{x}}_1)|^2 d\mathbf{x} = \epsilon_1^2 |H| > 0. \quad (3.5)$$

This will still hold when all the parameters are allowed to be changed simultaneously. The calculations becomes more messy, so we will not do so here, but geometrically, we can visualize two parabolas with different center and radius. It then becomes rather clear that these can not be equal at all sets larger than zero. Hence, we obtain that $\phi_2 - \phi_1$ is different from zero. Further, from the expression of $h_2 - h_1$, it then follows rather straightforward that there exists a domain of measure larger than zero where $h_2 \neq h_1$, and then clearly these are different in L^2-norm. Hence, we have in total that the operator S is one-to-one.

3.2 Nullspace of the forward operator

We have a one-to-one mapping from the subset D to the image $S(D)$ of the operator S. Hence, we must now prove that the mapping from $S(D)$, which is a subset of $H^1(H)$, onto the boundary of the body is one-to-one as well. This mapping was denoted above by a composition of three operators, namely $TL^{-1}Q$.

Let us assume that we have $h_1, h_2 \in S(D), h_1 \neq h_2$, where $S(D)$ is the image of the operator S, such that $TL^{-1}Q(h_1) = d = TL^{-1}Q(h_2)$. This will imply that $h_1 - h_2 \in \mathcal{N}(TL^{-1}Q)$ since $TL^{-1}Q$ is linear. But can this be true? Can we find two such elements in $S(D)$ such that the difference between them is in the nullspace of $TL^{-1}Q$. To answer this, we must find a way to describe this nullspace. However, this has already been done in [9].

Before we can use this nullspace we need to do some slight modifications to our forward operator. Initially, we did not have a unique solution to the problem (1.20), so we had to search for a solution in the subspace X (1.21). Then, our solution became unique. However, in [9], another uniqueness property is used, namely

$$\int_{\partial B} r \; dS = \int_{\partial B} d \; dS. \tag{3.6}$$

In [9], the authors argue that this provides the correct condition to optimize the least-squares solution. Hence, we will use this when implementing the inverse solver in the numerical section. But, to discuss this further now, we need to introduce some new operators. Let $K_1 : H^1(H) \longmapsto L^2(\partial B)$ be the same operator as the composition $TL^{-1}Q$ with the slight adjustment of uniqueness property. This operator is harder to use when discussing the nullspace, since this uniqueness property makes the mapping non-linear (the subset $\tilde{X} = \{u \in H^1(B) : \int_{\partial B} u = c \neq 0\}$ is not a true linear subspace of $H^1(B)$). Therefore, we also define the operator $K_2 : H^1(H) \longmapsto L^2(\partial B)$ as a solver of the same PDE, but with the uniqueness property $\int_{\partial B} r \; dS = 0$. Hence, we get $K_1(h) = K_2(h) + c$. Then, from [9], the nullspace of K_2 is described as

$$\mathcal{N}(K_2) = \{h(\Theta) \;:\; \Theta \in H_0^1(H) \text{ and h is a weak solution of (3.7-3.8)}\}$$

$$\nabla \cdot (M_i \nabla h) = -\nabla \cdot (M \nabla \Theta), \tag{3.7}$$

$$(M_i \nabla h) \cdot \mathbf{n_H} = -(M \nabla \Theta) \cdot \mathbf{n_H}. \tag{3.8}$$

But one justification remains. If $K_1(h_1) = d = K_1(h_2)$, does it imply that $h_1 - h_2 \in \mathcal{N}(K_2)$. Yes, this will be true since

$$K_1(h_1) = K_1(h_2) \Rightarrow K_2(h_1) + c = K_2(h_2) + c \Rightarrow K_2(h_1 - h_2) = 0. \tag{3.9}$$

So, what we must consider, is whether the overdetermined boundary value problem (3.10) has a weak solution.

$$\begin{aligned} -\nabla \cdot (M \nabla \Theta) &= \nabla \cdot (M_i \nabla (h_1 - h_2)), \text{ in } H. \\ \Theta &= 0 \text{ on } \partial H \\ -M \nabla \Theta \cdot \mathbf{n_H} &= M_i \nabla (h_1 - h_2) \mathbf{n_H} \text{ on } \partial H, \end{aligned} \tag{3.10}$$

where $h_1 \neq h_2$ and $h_1, h_2 \in S(D)$.

Now, since the conductivities are assumed to be uniformly elliptic, (3.10) would have a unique solution if we were given only the first boundary condition, but with the second as well, this is not very likely. The only way this could happen is if our solution happens to naturally have a gradient which coincide with the imposed one. We will try to describe whether this might be the case, and if we can find any requirements for our system to satisfy to avoid ending up in the nullspace. However, the next two subsections will discuss more general problems first, to illustrate how to deal with such problems.

3.3 Overdetermined Poisson operator

The problem we have reached now is in general hard to solve. Firstly, we have conductivities in the Poisson equation, and furthermore the right hand side is not non-negative nor non-positive over the domain, which makes this problem harder. But to highlight some of the techniques used to solve this for simpler overdetermined boundary value problems, we start of with

$$\begin{aligned} Lu &= f, \quad x \in \Omega \\ u &= 0, \quad x \in \partial\Omega \\ \frac{\partial u}{\partial n} &= 0, \quad x \in \partial\Omega, \end{aligned}$$

where L is a second-order elliptic operator. In addition, assume that $f(x) \leq 0$, $\forall\, x \in \Omega$, and f is smooth, such that we have a solution $u \in C^2(\Omega) \cap C(\bar{\Omega})$. In this case, given Ω is connected, open and bounded, and $Lu \leq 0$, the strong maximum principle implies that if u attains its maximum over $\bar{\Omega}$ at an interior point, then u is constant within Ω. If not, however, this implies that $u(x) < 0$, $\forall x \in \Omega$, from the Dirichlet condition. This again, is the same as saying that there exists a point $x_0 \in \partial\Omega$, such that $u(x_0) > u(x)$, $\forall x \in \Omega$, and thus we can apply Hopf's lemma [4], which then claims that $\frac{\partial u}{\partial n}(x_0) > 0$, and hence there is no solution to the overdetermined B.V.P.

In fact, from the article [10], there is a much more general existence property of elliptic partial differential equations. Given the PDE $Qu + f = 0$, such that $u > 0$ in Ω, where Q is a regular uniformly elliptic operator, along with the same boundary conditions as above, we can only have a classical solution to the problem if the domain Ω is a ball. Unfortunately, in our context, there is no guarantee that the solution will be positive throughout the domain, and must likely it will not, so we must find another approach to this problem.

3.4 Green's function for inhomogeneous Poisson's equation

We will try to get a better idea of the problem (3.10) by using Green's function. First, assume that we have the standard Poisson's equation

$$\begin{cases} -\Delta u = f, \ x \in \Omega \\ u = 0, \ x \in \partial\Omega. \end{cases}$$

This can be solved using the representation formula for Poisson's equation[4], which reads

$$u(x) = \int_\Omega G(x, x')f(x')\ dx', \tag{3.11}$$

where $G(x, x')$ is the Green's function for the Poisson's equation. When facing a slightly harder problem, with $-\nabla \cdot (c\nabla u) = f$ instead, where we assume that $c : \mathbb{R}^3 \longmapsto \mathbb{R}$, we can write $-\nabla \cdot (c\nabla u) = -\nabla c \cdot \nabla u - c\Delta u$. Thus, by rearranging, as done in [11], we get the following problem:

$$-\Delta u = \frac{f}{c} + \frac{\nabla c}{c} \cdot \nabla u = \frac{f}{c} + \nabla \ln(c) \cdot \nabla u. \tag{3.12}$$

Hence, we can write the solution as

$$u(x) = \int_\Omega G(x, x') \left[\frac{f(x')}{c(x')} + \nabla \ln(c(x')) \cdot \nabla u(x')\right] dx'. \tag{3.13}$$

Of course, this is a hard problem to solve, since the solution is inside the integral. However, if we had an overdetermined Poisson's equation with an additional homogeneous Neumann condition, we would only want to know if the derivative is equal to zero on the boundary, and since this variable is independent of the integral, we get

$$\frac{\partial u}{\partial n} = \int_\Omega \frac{\partial G}{\partial n_x}(x, x') \left[\frac{f(x')}{c(x')} + \nabla \ln(c(x')) \cdot \nabla u(x')\right] dx'. \tag{3.14}$$

If we could derive Green's function, we might have been able to tell something about the criteria for having a normal derivative equal to zero. Unfortunately, to find a Green's function is far from trivial, at least for complex geometries. So, we will try to determine the fundamental solution of $-\phi'' = \delta$ in $\mathbb{R}$ to get a better picture of what the solution of a simple overdetermined problem might look like.

To do so, we find the antiderivative twice and we get

$$\begin{aligned} &-\phi'' = \delta \\ \Rightarrow &-\phi' = H + C \\ \Rightarrow &-\phi = x_+ + Cx + D. \end{aligned} \tag{3.15}$$

where

$$x_+ = \begin{cases} x, & x \geq 0 \\ 0, & x < 0. \end{cases}$$

In addition, we want to make the solution symmetric and homogeneous. Hence, we get

$$-|x|(C+1) = C|x| - D \Rightarrow 2C = -1, \tag{3.16}$$

and $D = 0$. Thus, the solution reads

$$\phi(x) = -\frac{|x|}{2}. \tag{3.17}$$

From this, we can find the Green's function for the interval (0,1). The Green's function for Laplace's equation is defined by[4] $G(x, x') = \phi(x' - x) - \phi^x(x')$, $(x, x' \in \Omega, x \neq y)$. Here ϕ^x is a corrector function, which should satisfy

$$\begin{cases} \frac{d^2}{dx'^2}\phi^x = 0, & x' \in (0,1) \\ \phi^x = \phi(x' - x), & x' = 0, x' = 1. \end{cases}$$

This last condition implies that

$$\begin{aligned} \phi^x(0) = \phi(-x) &= -\frac{x}{2} \\ \phi^x(1) = \phi(1-x) &= -\frac{1-x}{2}. \end{aligned} \tag{3.18}$$

Further, since we have that $\frac{d^2}{dx'^2}\phi^x = 0$, then clearly $\phi^x(x') = Cx' + D$, and the boundary values implies that $D = -\frac{x}{2}$ and $C = x - \frac{1}{2}$. From this, we get that

$$\phi^x(x') = x'\left(x - \frac{1}{2}\right) - \frac{x}{2}, \tag{3.19}$$

and the Green's function will, by some calculations, become

$$G(x, x') = \begin{cases} x'(1-x), & x > x' \\ x(1-x'), & x \leq x'. \end{cases}$$

Then, we now want to use this Green's function to solve the equation $-\nabla \cdot (c\nabla u) = f$, using homogeneous Dirichlet conditions, which in 1D reads $-(cu')' = -cu'' - c'u' = f$. Thus, we have the following problem:

$$\begin{cases} -u'' = \frac{f}{c} + \frac{c'}{c}u' \\ u(0) = 0 = u(1). \end{cases}$$

Now, we can use the general result from above, and we get that

$$\begin{aligned} u(x) &= \int_0^1 G(x,y)\left(\frac{f}{c} + \ln(c)'u'\right)dy \\ &= (1-x)\int_0^x y\left(\frac{f}{c} + \ln(c)'u'\right)dy + x\int_x^1 (1-y)\left(\frac{f}{c} + \ln(c)'u'\right)dy. \end{aligned} \tag{3.20}$$

Note that we have used $x' = y$ to avoid confusion with the derivative signs. Also note that this will satisfy the homogeneous Dirichlet boundary conditions. If we add homogeneous Neumann conditions as well, to get an overdetermined system, the question whether a solution can still be obtained arises. Let us start our answer by taking the derivative of (3.20), to get

$$\begin{aligned} u'(x) = &- \int_0^x y \left(\frac{f}{c} + \ln(c)' u' \right) dy + (1-x)x \left(\frac{f}{c} + \ln(c)' u' \right) \\ &+ \int_x^1 (1-y) \left(\frac{f}{c} + \ln(c)' u' \right) dy - x(1-x) \left(\frac{f}{c} + \ln(c)' u' \right) \\ = &\int_x^1 (1-y) \left(\frac{f}{c} + \ln(c)' u' \right) dy - \int_0^x y \left(\frac{f}{c} + \ln(c)' u' \right) dy. \end{aligned} \quad (3.21)$$

This implies that

$$\begin{aligned} u'(0) &= \int_0^1 (1-y) \left(\frac{f}{c} + \ln(c)' u' \right) dy, \text{ and} \\ u'(1) &= - \int_0^1 y \left(\frac{f}{c} + \ln(c)' u' \right) dy. \end{aligned} \quad (3.22)$$

For $u'(0) = 0 = u'(1)$ to occur, then clearly we must have that

$$\int_0^1 (1-y) \left(\frac{f}{c} + \ln(c)' u' \right) dy = 0 = \int_0^1 y \left(\frac{f}{c} + \ln(c)' u' \right) dy. \quad (3.23)$$

In other words, both

$$\int_0^1 y \left(\frac{f}{c} + \ln(c)' u' \right) dy = 0, \quad (3.24)$$

and

$$\int_0^1 \left(\frac{f}{c} + \ln(c)' u' \right) dy = 0, \quad (3.25)$$

must be satisfied for this to be true. Hence, we observe that this will depend on the conductivity c. We might be unlucky enough to we have a conductivity where this is fulfilled. Nevertheless, this simple 1D example tells us how difficult it might be to solve such overdetermined problems. Therefore, we need to split the problem when we try to solve our original problem (3.10).

3.5 Sufficient uniqueness property

When we go back to the original overdetermined problem (3.10), we can describe this, using only the first boundary condition, as: Find $\Theta \in H_0^1(H)$ such that

$$\int_H \nabla\phi \cdot (M\nabla\Theta) dx = - \int_H \nabla\phi \cdot (M_i \nabla(h_1 - h_2)) dx, \quad \forall \phi \in H_0^1(H). \quad (3.26)$$

This has a unique solution in $H_0^1(H)$ from Riesz' representation theorem. Clearly, for (3.10) to be satisfied, this must hold. However, this solution Θ, must in addition be such that

$$-M\nabla\Theta \cdot \mathbf{n_H} = M_i\nabla(h_1 - h_2) \cdot \mathbf{n_H}. \tag{3.27}$$

Although it might be possible to describe a uniqueness demand in a more efficient manner than done here, we can at least conclude in the following theorem a sufficient condition for uniqueness:

Theorem - Uniqueness of forward operator. Let F be the forward operator from eq (1.63). If we have $\Theta(h_1, h_2)$ as solution of (3.26) such that

$$-M\nabla\Theta \cdot \mathbf{n_H} \neq M_i\nabla(h_1 - h_2) \cdot \mathbf{n_H}, \tag{3.28}$$

$\forall h_1, h_2 \in S(D)$, where $h_1 \neq h_2$, we will have a unique BSPM for each ischemic region.

Here as well, this seems to depend on the conductivities. If we can conclude that given this theorem holds, we will in fact have a continuous inverse throughout the entire parameter space $D \subset \mathbb{R}^4$, and thus the theoretical stability will hold for all BSPMs as well. From this, we leave the theoretical section, and move on to numerical work.

4 Numerical solution of forward problem

Going into this numerical section, we have some theoretical findings which might help us with the numerical work. We do know that a continuous forward operator exists, and we have a requirement for uniqueness. Thus, it might be an idea to implement a numerical solver which checks whether the requirement (3.28) is fulfilled or not. However, this will be quite some work, and it is not the main issue with this thesis, so we will not try to implement this here.

We know that we do not necessarily have a convex set, from the non-linearity of the forward operator, which might cause problems for the stability. This will be investigated in the inverse section. In addition, we changed the uniqueness property slightly when discussing the one-to-one mapping. From [9], eq (3.6) is argued to be the correct condition. Hence, we must take this into account when implementing our numerical solver. However, this new uniqueness property requires for the BSPM to already be known, and is therefore not very useful when creating a forward solver. Hence, we will first create the forward solver as discussed in section two, and instead find a way to incorporate the new uniqueness property when implementing the inverse solver.

4.1 General framework for finite element method

Before actually solving (1.27), we do need some framework for numerical solutions of partial differential equations: the finite element method. In abstract form, we might write a general elliptic PDE as: Let V be a Hilbert space. Let $a(\cdot,\cdot)$ be the weak form of a second-order elliptical partial differential equation, and $l \in V^*$. Find $u \in V$ such that

$$a(u, v) = l(v), \quad \forall v \in V. \tag{4.1}$$

For Poisson's equation with homogeneous Dirichlet conditions over the domain Ω, this would read: Find $u \in V$ such that

$$\int_{\Omega} \nabla u \cdot \nabla v \; dx = \int_{\Omega} f v \; dx, \quad \forall v \in H_0^1(\Omega). \tag{4.2}$$

In the finite element method, we create a finite dimensional subspace of V, called V_h, and search for a solution here instead. By making the ansatz that u can be approximated by $u_h = \sum_{j=1}^{N} u_j \phi_j$, where $\{\phi_j\}_{j=1}^{N}$ is a basis for V_h, it turns our problem into finding $u_h \in V_h$ such that

$$a(u_h, v) = l(v), \quad \forall v \in V_h. \tag{4.3}$$

And now, since we have made the ansatz, and of course only have to test against the basis functions, and not all v in V_h, since these in any case is just a linear combination of the basis functions, we get the following system:

$$\sum_j u_j a(\phi_j, \phi_i) = l(\phi_i), \tag{4.4}$$

which might be interpreted as a linear system $Au = b$, where $A_{ij} = a(\phi_j, \phi_i)$, and $b_i = l(\phi_i)$. Furthermore, since for a scalar u, we normally choose a space consisting of piecewise linear/quadratic/cubic etc functions(Lagrange elements), these only have support on a small part of the domain. Hence, we split the domain into small intervals/triangles/tetrahedrons, in 1D/2D/3D, and evaluate at each of these elements, and then map the solution into the global system. This is referred to as the local to global mapping. To do this, we assume that $a(u,v) = \sum_{T \in \mathcal{T}} a_T(u,v)$, where $\mathcal{T}$ is some triangularization of the domain. So, when we define the local matrix as

$$A_{ij}^T = a_T(\phi_j^T, \phi_i^T), \tag{4.5}$$

we only need the mapping to get from the local to global node. This mapping, however, will depend on the choice of basis function and triangularization.

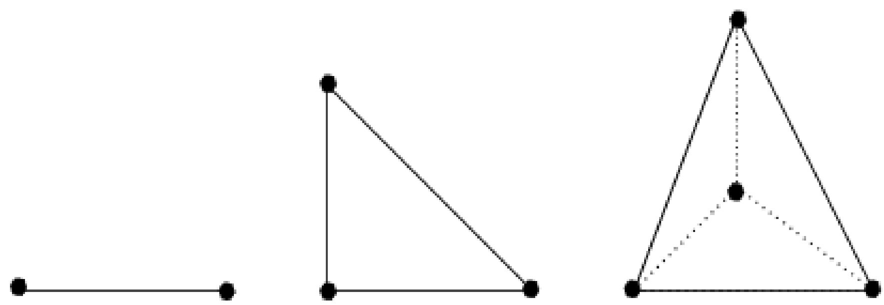

Figure 7: The triangular finite element with end point evaluation in 1D, 2D and 3D

Figure 7 gives us a geometric view of a triangle, and as said, the entire heart will be made up of such small elements.

4.2 Finite element formulation of forward problem

This powerful tool enables us to implement a solver, which takes the ischemic region as an input, and computes the recorded electrocardiogram. However, since we were facing a pure Neumann problem(1.20), we had to add a uniqueness property, which now requires us to do some modifications before we are able to incorporate the numerical finite element solution. On variational form (1.27), our problem reads: Find $u \in X = \{u \in H^1(B) : \int_B u = 0\}$ such that

$$\hat{L}(r, \psi) = \hat{Q}_h(\psi), \quad \forall \psi \in X. \tag{4.6}$$

But, since $\hat{L}(\cdot, \cdot)$ is symmetric and positive definite, this is equivalent to

$$\min_{\psi \in X} \left\{ \frac{1}{2} \hat{L}(\psi, \psi) - \hat{Q}_h(\psi) \right\} = \min_{\psi \in X} \hat{J}(\psi). \tag{4.7}$$

(See Proof 3 - Appendix A) This, however, can be redefined as

$$\min_{\psi \in H^1(B)} \hat{J}(\psi), \text{ such that } \int_B \psi = 0. \tag{4.8}$$

Hence, we can use the Lagrange multiplier, and get the optimality condition. However, to do so, we need a more general concept of a derivative:

Definition - Frechet derivative Let X and Y be Banach spaces. A continuous linear operator $P : X \longmapsto Y$ is said to be the Frechet derivative of $f : X \longmapsto Y$ at the point $x \in X$ if

$$f(x + h) = f(x) + Ph + \mathcal{O}(h) \text{ as } h \to 0, \tag{4.9}$$

or, equivalently

$$\lim_{h \to 0} \frac{\|f(x + h) - f(x) - Ph\|_Y}{\|h\|_X} = 0. \tag{4.10}$$

Hence, we see that for a linear functional, the derivative equals itself, since $f(x + h) = f(x) + f(h)$. So, we have the Lagrange conditions given by

$$\hat{J}'(\psi) = \gamma \left(\int_B \psi \, dx \right)' \tag{4.11}$$

$$\int_B \psi = 0. \tag{4.12}$$

We have already shown that the Frechet derivative of a linear operator is linear, so the derivative of the integral equals the integral, because this is a linear operator. So, we only have to consider $\hat{J}'(\psi)$. We start with

$$\begin{aligned}
\hat{J}(r + \psi) &= \frac{1}{2} \hat{L}(r + \psi, r + \psi) - \hat{Q}_h(r + \psi) \\
&= \frac{1}{2} \hat{L}(r, r + \psi) + \frac{1}{2} \hat{L}(\psi, r + \psi) - \hat{Q}_h(r + \psi) \\
&= \frac{1}{2} \hat{L}(r, r) + \hat{L}(r, \psi) + \frac{1}{2} \hat{L}(\psi, \psi) - \hat{Q}_h(r) - \hat{Q}_h(\psi) \\
&= \hat{J}(r) + \hat{L}(r, \psi) - \hat{Q}_h(\psi) + \mathcal{O}(\psi),
\end{aligned} \tag{4.13}$$

where $\mathcal{O}(\psi) = \frac{1}{2}\hat{L}(\psi, \psi)$ Hence, $\hat{J}'(r) = \hat{L}(r, \psi) - \hat{Q}_h(\psi)$, since

$$0 \leq \lim_{\psi \to 0} \frac{|\hat{J}(r + \psi) - \hat{J}(r) - \frac{1}{2}\hat{L}(\psi, \psi)|}{\|\psi\|_{H^1(B)}}$$
$$= \lim_{\psi \to 0} \frac{1}{2} \frac{|\hat{L}(\psi, \psi)|}{\|\psi\|_{H^1(B)}} \leq C \lim_{\psi \to 0} \frac{\|\psi\|^2_{H^1}}{\|\psi\|_{H^1(B)}} = 0. \quad (4.14)$$

Hence, we get the system: Find $(r, \gamma) \in H^1(B) \times \mathbb{R}$ such that

$$a(r, \psi) + \gamma \int_B \psi = \hat{L}(\psi), \quad \forall \psi \in H^1(B) \quad (4.15)$$

$$\sigma \int_B r = 0, \quad \forall \sigma \in \mathbb{R}. \quad (4.16)$$

From this, we are able to implement the solver. Now, since we are working in 2D, we will assume a really simple shape of the body and heart. With a geometry given as the unit circle, the innermost part will be the cavity of the heart, followed by the heart and then the torso. We will also use simple fiber structures for the conductivities. The extracellular conductivity in the heart will have a structure as shown in the figure below. The intracellular conductivities, along with the conductivities in the cavity and torso is assumed to be isotropic.

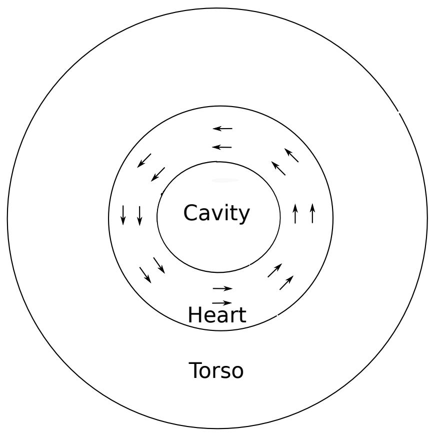

Figure 8: The shape of the fiber structures for the extracellular domain. In all other parts of the body, we assume simple isotropic conductivities.

We now have a formulation of our problem which can be implemented in numerical software, which will be done in the next subsection.

4.3 General implementation and forward solutions

To implement our solver, we have used a module in Python called DOLFIN. This is a part of the FEniCS Project, which is a collection of free software, designed for automated solutions of partial differential equations. Without this project, we would have to implement everything from scratch, which is fully doable, but would require much more work. However, before presenting a figure of some solutions of the forward solver, we will show how to implement the Poisson's equation with homogeneous Dirichlet conditions on the unit square (eg. 4.2) in the FEniCS framework.

```
#Import all functions from the module
from dolfin import *

#Create a mesh of size 50x50
mesh = UnitSquare(50,50)

#Define the function space of Lagrange-elements
#The number "1" means piecewise linear.
V = FunctionSpace(mesh, 'Lagrange', 1)

#Define the test- and trial functions
v = TestFunction(V)
u = TrialFunction(V)

#Define the right-hand-side function
#x[0] means the "x-variable", and
#x[1] the "y-variable".
f = Expression('cos(x[0])+x[1]')

#Define boundary function
u_bc = Constant(0)

#Check whether the point x is on the boundary
#If so, the on_boundary is True, so we might return
#this. If not, it is False.
def u_boundary(x, on_boundary):
    return on_boundary

#This is the boundary condition. We send the
#u_boundary in, to see which points returns true
#regarding if they are on the boundary.
bc = DirichletBC(V, u_bc, u_boundary)

#Compute the variational form of Poisson's eq.
a = inner(grad(u),grad(v))*dx
L = f*v*dx

#Compute the solution. a == L is the linear system
#to be solved. The solution vector is sent to u.
u = Function(V)
solve(a == L, u, bc)
```

This module makes our forward problem rather straightforward to implement. The right-hand side of (1.27), however, is rather messy, so we drop to add any more code. Instead, we present some solutions graphically in the figure below.

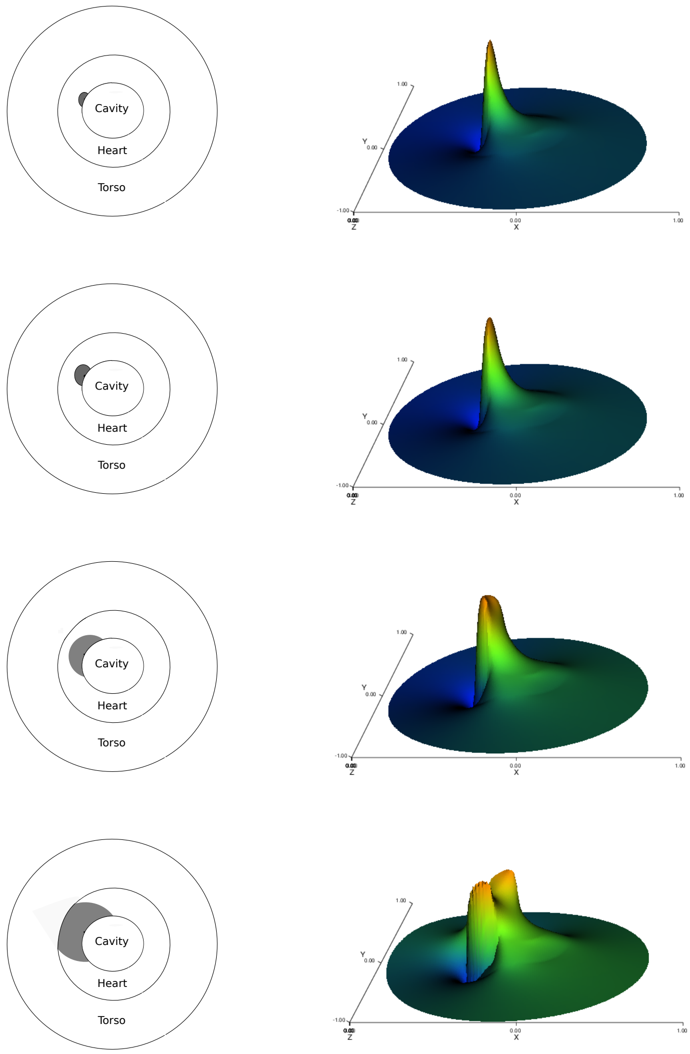

Figure 9: Evolving of a ischemic region and how it affects the extracellular potential

This forward solver is our starting point when we now turn to the inverse solver, since it will be used in the iteration process of trying to retrieve the ischemic region.

4.4 Visualization of cost-functional

Before we look at the inverse solver, we should try to get some idea of what the cost-functional looks like. If we fix the radius at the true value, and then make a 3D-plot of how the cost-functional looks with various coordinates for the center, we might get an idea about the possibility of retrieving the ischemic region from the recorded electrocardiogram.

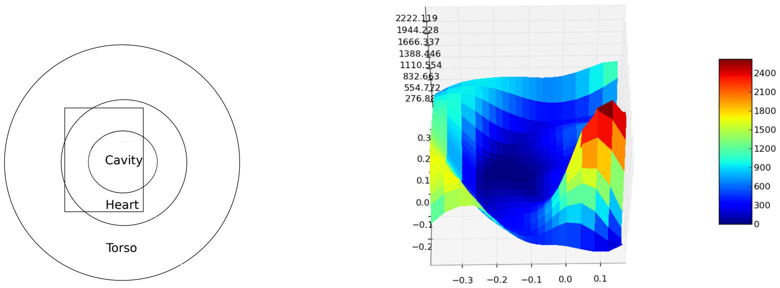

Figure 10: Looking at the cost-functional with a frozen radius. The rectangle in the left picture indicates the area where we computed the size of the cost-functional. The right picture is a 3D plot of these values. Observe that the cost-functional is not convex over this entire area, although it seems to be convex around the point $(-0.18, 0.087)$, which is the center of the ischemic region we used to compute the synthetic BSPM.

Now, we see that close to the center of the synthetic ischemic region, given as the point $(-0.18, 0.087)$, we have a steep descent, and will relatively easy manage to find this area using numerics. Unfortunately, we can see that farther away, this is not the case. On a larger domain, we do not have a convex cost-functional, not even when we freeze the radius, and only let the coordinates for the center be free, as done here. This will make our numerics harder, since we might end up in the wrong “dump” when searching for a minimizer of the cost-functional. Hence, we must find a way to deal with this, which will be discussed in the next section.

5 Inverse solution of electrocardiography

We have implemented a forward solver for the problem. Now, we want to make use of this forward solver to retrieve the ischemic region of a already known BSPM. This is in general a much harder task than solving the forward problem, and hence we must invoke some numerical iteration method to be able to do so. Therefore, we begin by explaining some useful algorithms for finding a minimum of a function.

5.1 Numerical methods for optimization

In the field of mathematical optimization, there is a vast number of techniques to use. In this text however, we will only introduce two popular methods, which we will use to solve the inverse problem. The first is a gradient descent method combined with a line search method, and the second is a penalty method, which also takes constraints into consideration. We might need this because we know from medicine that the ischemic heart disease starts at the endocardium.[2] Hence, it might be interesting to see what happens when we require the center of the ischemic region to be at the endocardium.

Method of steepest descent - This method is build around the fact that a function, $F : \mathbb{R}^n \longmapsto \mathbb{R}$, has its steepest descent in the direction of the negative gradient, i.e $-\nabla F$. If we take a step of appropriate length in this direction, we will get closer to the local minimum, which, for a convex function will be the same as a global minimum [26]. Thus, if we guess a solution x_0, we can make a algorithm as follows

Algorithm 2 The method of steepest descent

1: Guess some x_0
2: **repeat**
3: $\quad x_{k+1} = x_k - \gamma_k \nabla F(x_k)$
4: **until** $\|x_{x+1} - x_k\| < TOL$

This seems rather straightforward, but unfortunately, the way to choose γ_k is not trivial. If we make the steps to small, we will have a very poor convergence rate, and on the other hand, if we make the steps to large, we might "overshoot" the step, and get out of the interesting area. One remedy for this, is to check the Wolfe conditions [12], which is given by two inequalities:

[2] Endocardium is the innermost tissue, lining the chambers of the heart.

The Wolfe conditions:

$$F(x_k + \gamma_k p_k) \leq F(x_k) + c_1 \gamma_k \nabla F(x_k)^T p_k \tag{5.1}$$
$$\nabla F(x_k + \gamma_k p_k)^T p_k \geq c_2 \nabla F(x_k)^T p_k, \tag{5.2}$$

where $p_k = -B_k^{-1} \nabla F(x_k)$ for some positive definite B_k^{-1}. Then p_k turns out to be a descent direction since $\nabla F(x_k)^T p_k < 0$. If we set $B_k^{-1} = I$, we obtain the steepest descent.

Further, $c_1 \in (0, 1)$ and $c_2 \in (c_1, 1)$. The first Wolfe condition (5.1) is often referred to as *Armijo condition*, which makes sure that the decrease if sufficient. In other words, since $\nabla F_k^T p_k < 0$, inequality (5.1) requires the decrease to be larger than some scaling c_1 of the decrease direction and length.

The second condition (5.2), known as the *curvature condition*, stops us from making the steps to small: By defining $m_k : \mathbb{R} \longmapsto \mathbb{R}$ by

$$m_k(\gamma) = F(x_k + \gamma p_k), \tag{5.3}$$

we get $m_k'(\gamma) = \nabla F(x_k + \gamma p_k)^T p_k$ from the chain rule. Hence, $m_k'(0) = \nabla F(x_k)^T p_k$, which is equal to the right-hand side of inequality (5.2) when we disregard c_2. The *curvature condition* tells us in fact that the decrease of $m_k(\gamma)$ at y_k should be less negative than some scaling c_2 of the decrease $m_k'(0)$. In other words, the second criterion states that if the slope at γ_k is very negative, we should take a bigger step in the direction of p_k.

Having explained these conditions roughly, we will now post a theorem from [26], which provides us with some convergence property of a sequence satisfying Wolfe conditions:

Theorem - Convergence with Wolfe conditions Let some iteration process be given by $x_{k+1} = x_k + \gamma_k p_k$, where p_k is the descent direction and γ_k satisfies the Wolfe conditions above. Suppose that F is bounded below in $\mathbb{R}^n$ and that $F \in C^1(\mathcal{N})$, where $\mathcal{N}$ is a open set containing $\mathcal{L} = \{x \mid f(x) \leq f(x_0)\}$, where x_0 is the initial guess. In addition, assume that the gradient ∇F is Lipschitz continuous on $\mathcal{N}$. Then

$$\sum_{k \geq 0} \cos^2(\theta_k) \|\nabla F_k\|^2 \leq \infty, \tag{5.4}$$

where $\cos(\theta_k)$ is defined as

$$\cos(\theta_k) = \frac{-\nabla F_k^T p_k}{\|\nabla F_k\| \|p_k\|}. \tag{5.5}$$

When p_k is equal to the steepest descent, clearly $\cos(\theta_k) = 1$. Hence, it follows from (5.4) that

$$\lim_{k \longmapsto \infty} \|\nabla F_k\| = 0. \tag{5.6}$$

In other words, we can be sure to converge to some stationary point. We can not, however, be sure that this is a minimizer.

To check these two criteria making up the Wolfe conditions (5.1-5,2), we must once more find a numerical algorithm. One remedy is to implement the backtracking line search[13]. The idea is to start with a large enough step size to make sure that the curvature condition is met, and then we make the decrease sufficient by the following

Algorithm 3 Backtracking line search

Choose some $\alpha > 0, \tau, c \in (0,1)$
repeat
  $\alpha \leftarrow \tau\alpha$
until $F(x_k + \alpha p_k) \leq F(x_k) + c\alpha \nabla F(x_k)^T p_k$
End with $\gamma_k = \alpha$

This method does often work, but as mentioned earlier, it does not take constraints into consideration. Hence, we will now introduce the penalty method. What we do then, is to define a penalty function, which basically "punishes" the objective function by increasing the value if we get outside the set of valid inputs, and thus sends us back into this set.

Penalty method - Hence, the idea is to add a extra term on the function we want to minimize, and increase the value of this function as we get farther away from our given set of input parameters. For example, if we want to minimize a function $f : \mathbb{R}^n \longmapsto \mathbb{R}$ together with a constraint $c : \mathbb{R}^n \longmapsto \mathbb{R}$, given by

$$\begin{aligned} \min_x \quad & f(x) \\ \text{such that} \quad & c(x) = 0, \end{aligned}$$

we must find a way to take this constraint into account. This can be done by introducing the penalty method

$$\phi(x;\mu) = f(x) + \frac{1}{2\mu} c^2(x), \tag{5.7}$$

for some $\mu \in \mathbb{R}_+$, and then try to find $\min_x \phi$ using a unconstrained minimization method, like steepest descent. Before we can implement the algorithm, however, we must figure out how to deal with the newly introduced μ. From (5.7), we see that when we reduce this number, the penalty term gets a bigger influence on the total sum. Therefore, it makes sense to make a decreasing positive sequence $\{\mu_k\}$, and find the optimal x_i^* for μ_i, and use this as a start guess for μ_{i+1}, where $\mu_{i+1} < \mu_i$. Doing so, the algorithm becomes:

Algorithm 4 Penalty method

```
Choose some μ_0 > 0, a decreasing sequence {τ_k} converging to zero, and
an initial point x_0^i ∈ R^n
for k = 0, 1, 2, ... do
    Solve min φ(x; μ_k), starting at x_k^l with the convergence criterion
    ‖∇_x φ(x; μ_k)‖ ≤ τ_k. Denote this solution by x_k.
    if the outer convergence test is satisfied then
        stop with the approximate solution x_k.
    end if
    Choose new penalty parameter μ_{k+1} < μ_k.
    Choose new starting point x_{k+1}^i.
end for
```

We see that by combining these methods, we can make a inverse solver for our system. However, before we do so, we must remember that our forward solver used the wrong uniqueness property, and hence we will now argue how we can modify this condition when trying to solve the inverse problem.

5.2 From wrong to right uniqueness property for the inverse solver

In the last chapter, we made a solver to the problem: Find $r \in H^1(B)$ such that

$$\int_B \nabla v \cdot (M \nabla r) dx = - \int_H \nabla v \cdot (M_i \nabla h) dx, \quad \forall v \in H^1(B),$$
$$\int_B r \ dx = 0. \tag{5.8}$$

But, from the last theorem of Chapter 3 (3.28), we needed a different uniqueness property (3.6). Hence, we need to find a way to take this into account. Let $\bar{r} \in H^1(B)$ be the solution to the PDE (1.27) with the new uniqueness property. However, since the PDE with a homogeneous Neumann conditions is unique up to a constant, it follows that

$$\bar{r} = r + c, \tag{5.9}$$

where c is a constant and r is the solution of (5.8). This implies that

$$\int_{\partial B} \bar{r}\; dS = \int_{\partial B} r\; dS + \int_{\partial B} c\; dS$$
$$\Rightarrow c = \frac{\int_{\partial B} d\; dS - \int_{\partial B} r\; dS}{|\partial B|}. \tag{5.10}$$

The idea with the inverse solver is to solve the optimality system (1.60). Thus, we need the gradient of $J(x_0, y_0, z_0, s)$ from (1.40). We computed this for $\frac{\partial J}{\partial x_0}$ and $\frac{\partial J}{\partial s}$ in (1.58)-(1.59), and more generally it reads

$$\tilde{\nabla} J = \int_{\partial B} (\bar{r} - d)\tilde{\nabla}\bar{r}. \tag{5.11}$$

Thus, when we combine this with (5.9-5.10), we get

$$\tilde{\nabla} J = \int_{\partial B} (\bar{r} - d)\tilde{\nabla}\bar{r} = \int_{\partial B} (r + c - d)\tilde{\nabla}\bar{r}. \tag{5.12}$$

One question remains, and that is how to compute $\tilde{\nabla}\bar{r}$. We have that $\bar{r} = r + c$, but remember that this c is a constant with respect to the vector-valued variable representing the position in the heart, and not with respect to the set of parameter variables (and it is this gradient we compute). Hence, we have

$$\tilde{\nabla}\bar{r} = \tilde{\nabla}(r + c) = \tilde{\nabla} r + \tilde{\nabla} c = \tilde{\nabla} r - \frac{1}{|\partial B|}\int_{\partial B} \tilde{\nabla} r\; dS, \tag{5.13}$$

where the last equality follows from (5.10). Hence, we do not have to solve more equations numerically. Instead, we only have to compute the value for the constant c, and do this small trick to the cost-functional, which should not cause any problems.

5.3 Inverse solution for BSPM in the image of the forward operator

With this correct uniqueness property, we can try to solve the inverse problem. We did find, however, that since the forward operator F is non-linear, we will probably not have a convex image, which can cause problems with the continuity of the least-squares solution. Furthermore, we saw from Figure 10 that the cost-functional is in fact not a convex function either. When doing optimization with non-convex functions, we might run into problems. That is, if we start in the wrong "dump", we will not find the global, but only a local minimum. One remedy is to start our initial guess at several different locations in the heart, and then run the forward solver with the solutions found from the inverse solver, to find which produces the forward solution closest in norm to the BSPM. Also, we might make use of the fact that ischemic heart disease evolves from the endocardium, and thus add a constraint which takes this into account. Mathematically, such a constraint would read

$$c(x, y, z) = (x - x_0)^2 + (y - y_0)^2 + (z - z_0)^2 - r_0^2 = 0, \qquad (5.14)$$

where r_0 is the radius of the cavity from Figure 8. In our computations, $r_0 = 0.2$. If we add this constraint, and use the penalty method to solve the problem, we might converge to the optimal solution with a worse initial guess than would be applicable to the unconstrained solver.

However, let us first try to solve the inverse problem with the simplest - the unconstrained - method. In the previous chapter, we made some forward solutions (see Figure 9), and we will now use one of these synthetic BSPMs to run the inverse solver. The third simulation in Figure 9 has an ischemic region represented by the center $(-0.18, 0.087)$ and radius 0.14. In all the following simulations, we make use of 42 electrodes on the surface of the body. Also, the findings will be presented in tables and figures. The first table shows the iteration process of retrieving the ischemic region mentioned above.

Table 1: Iteration with good initial guess

#	x_0	y_0	s
0	-0.20000	0.20000	0.10000
1	-0.15879	0.15617	0.11164
2	-0.17218	0.12149	0.17448
3	-0.18717	0.12800	0.16748
4	-0.16535	0.10295	0.14144
5	-0.18434	0.07169	0.14115
10	-0.18315	0.08521	0.13871
15	-0.18207	0.08741	0.13935
19	-0.18182	0.08739	0.13987

In the table above, we can observe that the inverse solver terminates close to the true ischemic region given by $(-0.18, 0.087, 0.14)$. In this first run, however, we "guessed" an initial starting point for the iteration relatively close to the true ischemic region. Because of the non-convex cost-functional, we might expect trouble when we use a worse initial guess.

The table on the next page does confirm our suspicion: When starting farther off, we were not able to converge to the true solution. Due to the non-convexity, we did end up in the wrong "dump". Therefore, it is natural as a next step to incorporate the inverse solver with the penalty method with the extra term $c^2(x, y, z)$, where c is from eq (5.14), to check whether this method provides better results. We can in this case observe from Table 2 that we were able to solve the inverse problem. Hence, it seems like our penalty solver might be more robust. Note that "n/a" in Table 2 merely means that we have reached the converge criterion.

Table 2: Iteration with worse initial guess - two methods

	without constraint			with constraint (5.14)		
#	x_0	y_0	s	x_0	y_0	s
0	-0.20000	-0.20000	0.10000	-0.20000	-0.20000	0.10000
1	-0.16131	-0.16588	0.09635	-0.13258	-0.14052	0.09368
2	-0.15346	-0.13938	0.06802	-0.15088	-0.08624	0.04565
3	-0.14939	-0.11619	0.08612	-0.18807	-0.09169	0.12493
4	-0.14954	-0.10959	0.08616	-0.19947	-0.07736	0.05490
5	-0.14929	-0.10363	0.08694	-0.15422	-0.54166	0.12932
10	-0.14933	-0.10059	0.08759	-0.15559	-0.05416	0.09845
15	-0.14934	-0.10048	0.08762	-0.16564	0.02337	0.12705
20	n/a	n/a	n/a	-0.17005	0.07671	0.13539
30	n/a	n/a	n/a	-0.17156	0.08300	0.13870
40	n/a	n/a	n/a	-0.17592	0.08490	0.13857
50	n/a	n/a	n/a	-0.17730	0.08571	0.13929
88	n/a	n/a	n/a	-0.17928	0.08667	0.13995

In Table 1, when we started close to the true ischemic region, we found an inverse solution close to this true ischemic region, using the unconstrained solver. As Table 2 shows, however, this was not the case when we started farther off. We did suggest a remedy for the non-convexity earlier; start at several locations, and insert the inverse solutions as parameters in the forward solver, before taking the norm between these generated forward solutions and the BSPM. Finally, choose the inverse solution providing the smallest distance from the BSPM.

Entering the two regions we obtained from the unconstrained inverse solver (Table 1 and left part of Table 2) into the forward solver gave us distances from the BSPM of 0.0017 and 120.3082 respectively when applying the $\mathbb{R}^{42}$-norm. From the strategy we suggested in the beginning of this subchapter, we then pick the solution from Table 1.

5.4 Ischemic region as a square

Moving on from the trivial case of a circle-shaped ischemic region, we will now step outside the image of the forward operator, by representing the true ischemic region with a different geometry. We will solve the forward problem with the ischemic region represented as a square. However, to do so, we need to make some modifications to the mapping from the center and radius into the Heavside-function(1.45).

We still want a function which takes negative values inside the ischemic region, and positive outside. However, with a square-shaped region, we need a different function. We know that using the infinity norm in $\mathbb{R}^2$, the "unit-ball" is shaped like a square. Using this as a start, we suggest the function

$$\phi = \max(|x - x_0|, |y - y_0|) - s, \tag{5.15}$$

which takes positive values outside the square in Figure 11, and negative values inside. However, it is not quite straightforward to compute the derivative of this function, since this will depend strongly on the part of the domain we are in. To sort this out, we make use of the figure.

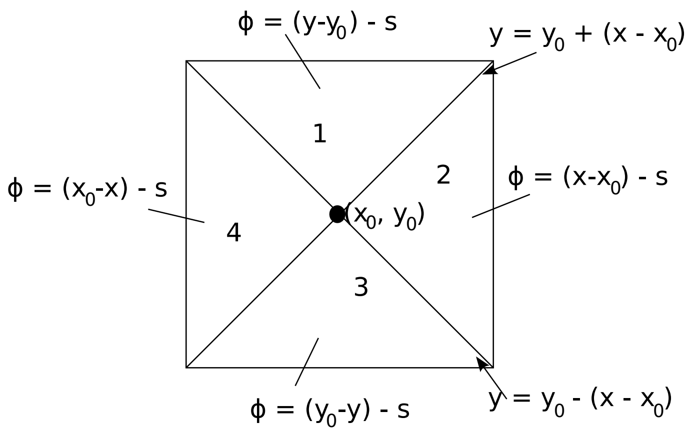

Figure 11: The ischemic mapping as a square

With this visualization, it is quite trivial to solve the derivative:

$$\frac{\partial \phi}{\partial x_0} = \begin{cases} 0, & \text{x in region 1 and 3} \\ 1, & \text{x in region 2} \\ -1, & \text{x in region 4,} \end{cases}$$

and similarly,

$$\frac{\partial \phi}{\partial y_0} = \begin{cases} 0, & \text{x in region 2 and 4} \\ 1, & \text{x in region 1} \\ -1, & \text{x in region 3.} \end{cases}$$

Now, we can implement this in the forward solver, and produce a synthetic "true" BSPM. When starting the inverse process, we will then hopefully converge to a circle which approximates the square quite well. We create two different square-shaped regions, as shown in Figure 12. The left part has a center in (-0.17, -0.105) with a "radius" of 0.12.

Figure 12: Two different square-shaped ischemic regions

We see from Table 3 below that we needed many more iterations. This is probably due to the fact that we have moved outside the image of the forward operator. Hence, the steepest descent, which is a rather simple method, has problem with convergence (the convergence rate of steepest descent is only linear[26]). However, what we observe from the solution, is that the solution is approximating the square quite well. It might be hard to see this from the numbers, when the radius is not directly comparable between the circle and the square, but Figure 13 provides a much better visualization of the solution. Therefore, we will not include more iteration tables, but instead focus on the figures, since these provide a better visualization when using ischemic regions with other shapes than circles.

Table 3: First attempt to approximate a square with a circle

#	x_0	y_0	s
0	-0.20000	-0.20000	0.10000
1	-0.14453	-0.14646	0.10069
2	-0.13980	-0.13495	0.12869
3	-0.14297	-0.13396	0.10604
4	-0.14201	-0.12895	0.12490
5	-0.14453	-0.12881	0.10926
10	-0.14630	-0.12324	0.11794
20	-0.14991	-0.12157	0.11695
40	-0.15418	-0.12130	0.11638
60	-0.15580	-0.12127	0.11573
80	-0.15643	-0.12128	0.11560
100	-0.15665	-0.12140	0.11523
255	-0.15664	-0.12129	0.11567

As mentioned, the circle provides a good approximation to the square, as seen in Figure 13. Note that we have zoomed in on the body here, and only focus on the left-side of the heart. So, we only see the ischemic regions and the cavity wall of the heart.

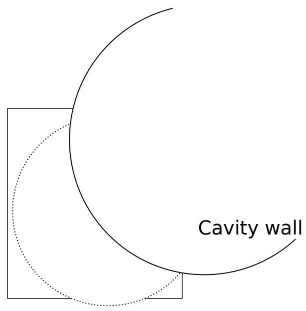

Figure 13: The circle from the inverse solution of square-shaped region together with the true region

Since we have the forward solver for both of the regions in Figure 13, we might run them once more in the forward solver, and then plot them to see how they compare.

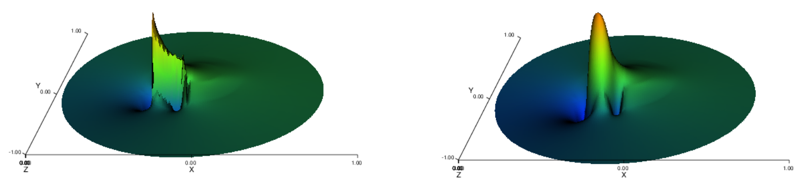

Figure 14: The forward solution of square and circle corresponding to the ischemic region of the previous figure.

We can see that these two are quite similar on a large scale, with the exception of the peak formed as a square and a circle, respectively. The values they take at the boundary, however, is not clear from Figure 14. But when measuring the relative distance

$$\delta = \frac{\|\text{BSPM}_{square} - \text{BSPM}_{circle}\|}{\|\text{BSPM}_{square}\|}, \tag{5.16}$$

this takes the value 0.0155. In other words, we have a relatively good approximation.

The second square-shaped ischemic region had a placement of $(-0.06, 0.19)$, and a radius 0.12 (see right panel in Figure 12). From Figure 15, we see that the inverse solution is close in this case as well. However, the inverse solutions in both Figure 13 and Figure 15 requires us to start in the right quadrant, in the same way as with the circle-shaped ischemic region. Hence, we must follow the same recipe as before, and start iterating with several initial guesses. When doing so, however, we seem to get good approximations.

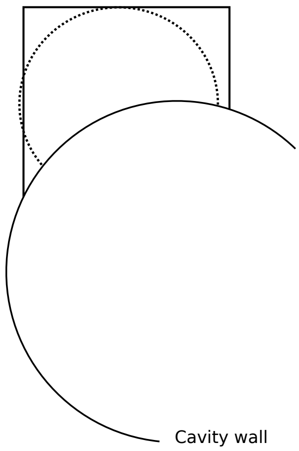

Figure 15: The solution of the inverse solver together with the second square-shaped ischemic region.

Creating square-shaped ischemic regions was one possible way of checking the robustness of our inverse solver. A more common path is to add noise to the synthetic data we produced from the forward solver. That is, we use the forward solver, and apply some algorithm to add noise to the output we get. This will be done in the next subsection.

5.5 Adding noise to our synthetic data

As mentioned, adding noise to the synthetic data is a widely used method to check the robustness of the inverse solver. Often, we use something called Gaussian white noise. That is variables from the normal distribution with zero mean and standard deviation, i.e $(\mu, \sigma) = (0, 1)$. We add a randomly generated number from this distribution to each of the numbers in the electrocardiogram. But, before we do so, we will illustrate the white noise process by an example.

Example 5.1 (Adding noise to a function) Let $f : [0, 2\pi] \longmapsto \mathbb{R}$ be a function defined by

$$f(x) = \cos(x), \tag{5.17}$$

and add 10% noise to this function.

To accomplish this, we use a Python function which draws random numbers from the normal distribution, then scale it by 0.1(to get 10 % noise), and add to the function. We then get the following plot:

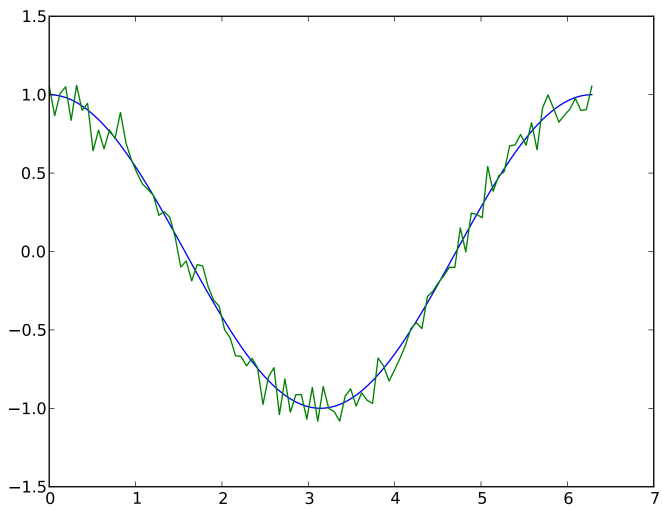

Figure 16: Adding 10% noise to the function $f(x) = \cos(x)$.

Now, we can use the same method to add noise to the synthetic BSPMs. At each of the electrodes we add a number randomly chosen by the standard distribution. We start by 10%, as in the example, and then add more noise later, to see how this affects the ischemic region computed with the inverse solver.

As shown in the Figure 17, adding noise does not affect the ischemic region to a great extent. All four tested levels of noise is well dealt with by the inverse solver. This speaks in favor of our theoretically proven stability also being useful for numerical purposes. Of course, this is to early to say something solid about after just a few test runs, but we will address this issue more in the last chapter.

In addition to obtaining good results when adding noise, the number of iterations is not much affected either. With 10 and 20% noise, there is actually no difference in the number of iterations used, but it increases from 19 iterations without noise (Table 1) to 32 iterations when we add 50% noise.

It seems that our inverse solver is rather robust. When working in real life, however, we will have a limited number of electrodes to measure the BSPM. Hence, it might be interesting to see how the inverse solver behaves when we reduce the number of electrodes. As mentioned in the beginning of this chapter, we have up until now used 42 electrodes, but this will now be reduced in the forthcoming subchapter.

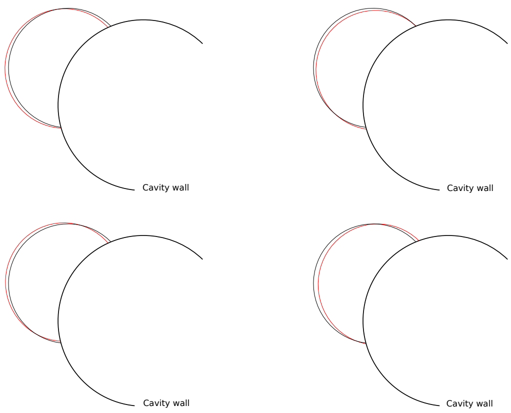

Figure 17: The effect of adding noise. The black circle represent the true ischemic region, and the red circles are the inverse solutions after adding 10, 20, 30 and 50 % noise respectively.

5.6 Reducing the number of electrodes

What we will do now, is to re-run some of the previous experiments with a reduced number of electrodes, first to 21, then down to 10 electrodes before testing with only 4 electrodes.

Before testing with noise, however, we will just run the simple case of having a circle-shaped ischemic region. We will not show a figure of these results, but only say that when using 21 electrodes, we got an inverse solution with center (-0.1776, 0.0859) and a radius of 0.1396, when using 10 electrodes, the center was (-0.1753, 0.0841) with a radius of 0.1394 and when using 4 electrodes the center was (-0.1846, 0.0892) with a radius of 0.1398. Hence, all three were close to the true ischemic region of center (-0.18, 0.087) and a radius of 0.14. It seems that reducing the number of electrodes does not greatly affect our ability to get close to the true solution when applying our inverse algorithm.

In the last subchapter, we observed that the ischemic regions found from the inverse solver were close to the real ischemic regions even when adding noise. When reducing the amount of electrodes we might suspect inverse solutions farther away from the true solution due to more sensitivity to the noise with fewer electrodes.

When reducing the number of electrodes to 21, this does not seem to be the case, looking at Figure 18. When adding 10 % noise, our inverse solution is relatively close to the solution we had without any reduction in electrodes. This also seems to be the case with 30% noise.

When reducing even further, to 10 electrodes, we can see that the first solution is overestimating the size of the ischemic region to some extent. There might be several reasons for this. The reduction of electrodes might have caused greater sensitivity to noise, or the noise might not be random enough with so few draws from the normal distribution. When increasing the noise, however, we did not overestimate the size of the ischemic region, which might suggest that it was just coincidence causing the overestimate with 10 % noise.

Finally, when reducing down two 4 electrodes, we still obtain inverse solutions close to the true ischemic region. This time, on the contrary to when we had 10 electrodes, the best solution is obtained with 10% noise. With 30% noise, we see that the center is somewhat shifted away from the true center, but still, we obtain fairly good results. This supports our stability.

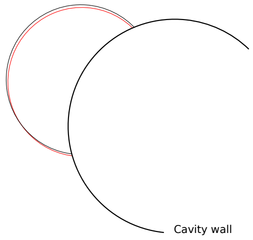

(a) Inverse solution using 21 electrodes and adding 10% noise.

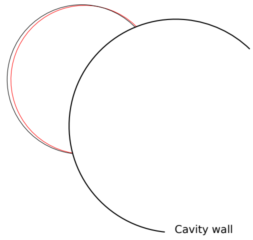

(b) Inverse solution using 21 electrodes and adding 30% noise.

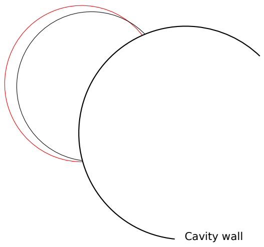

(c) Inverse solution using 10 electrodes and adding 10% noise.

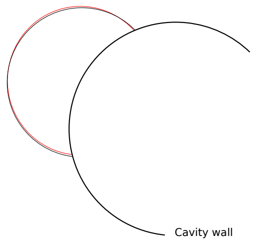

(d) Inverse solution using 10 electrodes and adding 30% noise.

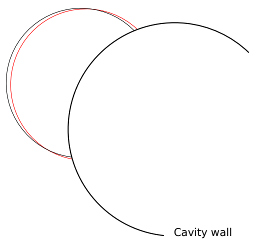

(e) Inverse solution using 4 electrodes and adding 10% noise.

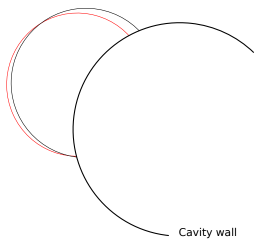

(f) Inverse solution using 4 electrodes and adding 30% noise.

Figure 18: True ischemic regions are displayed with black circles, while inverse solutions from the synthetic BSPMs are displayed with red circles. The caption under each picture states the amount of noise and number of electrodes used.

6 Conclusions and future perspective

When we started this thesis, we highlighted some of the problems with the inverse problem of electrocardiography. Even though some regularization had shown some progress, it was still a big task to get the instability under control. In the theory section of this thesis, we did prove a continuous forward mapping, and also a continuous inverse as long as the last theorem of Chapter 3 holds, i.e

$$-M\nabla\Theta \cdot \mathbf{n_H} \neq M_i\nabla(h_1 - h_2) \cdot \mathbf{n_H}, \quad \forall h_1, h_2 \in S(D), h_1 \neq h_2. \tag{6.1}$$

If this is true, will probably depend on the conductivities, and when moving to real-life applications, it might be beneficial to incorporate a quick integrator which specifically checks if eq (6.1) is satisfied. However, we do not know how strong the stability is. In fact, it might be only a theoretical stability. To explain what we mean by that, we will consider the a linear problem

$$Lu = f. \tag{6.2}$$

When we discretize this into a linear algebra problem, it will read

$$Ax = d. \tag{6.3}$$

Now, we would like to solve (6.3). In real life, however, we normally have noise in our measurements. Referring to the problem discussed throughout this thesis, we can relate d to the potential over the body, and x is some parameterization of the ischemic region. Using the electrocardiogram, however, implies that we get noise in our data, so the problem becomes

$$Ax^* = d + d_{noise} = d_{ECG}. \tag{6.4}$$

But, even though we normally have some noise in our data, we might find good solutions, depending on the matrix A. To understand this further, let us look at the relative error

$$\begin{aligned}
&\frac{\frac{\|x^*-x\|}{\|x\|}}{\frac{\|d_{noise}\|}{\|d\|}} = \frac{\frac{\|\Delta x\|}{\|x\|}}{\frac{\|d_{noise}\|}{\|d\|}} = \frac{\frac{\|A^{-1}d_{noise}\|}{\|A^{-1}d\|}}{\frac{\|d_{noise}\|}{\|d\|}} = \frac{\|A^{-1}d_{noise}\|}{\|d_{noise}\|}\frac{\|d\|}{\|A^{-1}d\|} \\
&\frac{\|A^{-1}d_{noise}\|}{\|d_{noise}\|}\frac{\|Ax\|}{\|x\|} \leq \frac{\|A^{-1}\|\|d_{noise}\|}{\|d_{noise}\|}\frac{\|A\|\|x\|}{\|x\|} = \|A\|\|A^{-1}\| = \kappa(A),
\end{aligned} \tag{6.5}$$

where $\kappa(A) = \|A\|\|A^{-1}\|$ is the condition number of the matrix. Hence, the condition number tells us how large the error is the solution can be in ratio to the relative noise. Thus, if the matrix A has a small condition number, the error in the solution will be relatively small. Unfortunately, we can only find the condition number of a linear system, and since the operator F

(1.63) is non-linear, it can not be represented as a linear system. For non-linear systems, there is no general method for measuring the relative error. One remedy might be to linearize the system, but that will not work well for strongly non-linear systems. Therefore, we should try and classify the non-linearity of the system, and then find an algorithm to determine how large the relative error is, depending on the non-linearity. This task might become rather difficult.

Even though we might have uniqueness of the forward operator, we do not know what happens outside the forward image. Since we have reduced the space of ischemic regions to only circles, we have also reduced the image of the forward operator, and outside here, we do now know much about continuity. The stability gained by reducing the ischemic space might only apply inside the image of the forward operator. Hence, we might still have instability outside the image of the forward operator. However, we did not experience anything like this when adding noise, nor when we had a square-shaped ischemic region. This might support that the stability found in the theoretical section does apply in some of the area outside this image(see Figure 6).

Another interesting fact about the continuity, was the relation between the Lipschitz continuity and the size of the transition zone. During the proof of continuity of the forward operator (Theorem 1 - Chapter 2), we saw that most of the terms in the inequality was dependent on the reciprocal of the size of the transition zone. Hence, it might be interesting to see whether this parameter will have a real influence on the ability to handle noise well.

When we moved to the numerical section, we decided to work with a 2D heart. This was mainly due to visualization simplifications. Obviously, in the next phase, we should expand the work to 3D. Then, we should also incorporate more real-life tensors for the heart. Of course, this must come from research. Also, the work must be compared to data from real patients to make us able to determine how well this will work in real life.

A somewhat surprising effect was the section on reduced number of electrodes. Reducing the number of electrodes to half, did not seem to have any practical impact on the inverse solution, even with adding noise. This might suggest that we were still able to capture all the major attributes of the BSPM. Also, when reducing the electrodes even more, we still managed to get rather good solutions. This is promising, and might suggest that our method does not require to many electrodes when trying to determine an ischemic region. However, since we are working in 2D now, this might not be the case when expanding the work to 3D. Hence, this should be tested more thoroughly then. Nevertheless, we seem to get quite promising results regarding the stability of our solution.

We also did some some simulations with the penalty method. This made the solver more robust since we got convergence to the true solution with poor starting guesses, which did not succeed without the penalty method (cf. Table 2). However, we did then operate in the image of the forward operator. In real life, on the other hand, we might get ischemic regions where it would make little sense to force the center of the ball to lie on the endocardium (see Figure 19). Thus, we should be careful to implement this in a real-life solver, even though it seems to give us more robustness. Besides, even though we could be more sloppy with our start guess when using the penalty solver, we have already mentioned one remedy for this: Start at several locations and pick the solution giving the forward solution closest to the BSPM. Another possibility might be to apply the penalty method to a random initial guess, and using the solution from this method as a starting point for the unrestricted method. Hopefully the penalty method then has gotten us into the valid area for the unconstrained solver.

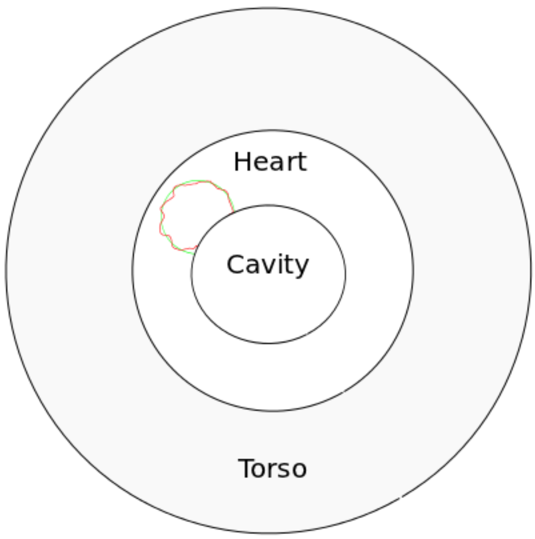

Figure 19: The true ischemic region in red, and a possible approximation with a ball which is not centered at endocardium in green.

Hence, in total we found some promising results, but we have pointed out some weaknesses which ought to be analyzed further. If these weaknesses should work out, and we get promising results with real data, we might also want to look at a GUI (Graphical User Interface), and it might be useful to move from Python to C++ to gain some speed in the iteration process. Already, a lot of the methods in FeniCs are being swapped to C, but probably there might be possible to reduce the computing time because of all the iterations in the inverse solver. In addition, we should incorporate a more sophisticated inverse solver than the steepest descent, e.g, a trust-region method, to acquire a quadratic convergence rate[26]. This to reduce the number of iterations we needed in some of the cases (e.g, the square-shaped region, cf. Table 3).

References

[1] A. J. Pullan, M.L. Buist and L. K. Cheng. *Mathematically modeling the electrical activity of the heart: From cell to body surface and back again.* World Scientific Publishing Company, Singapore 1st Edition, 2005.

[2] B. F. Nielsen, O. M. Lysaker, P. Grøttum, K. A. Mardal, A. Tveito, C. Tarrou, K. Haugaa, A. Abildgaard, and J. G. Fjeld. *Can ECG recordings and mathematics tell the condition of your heart?.* In A. Tveito, A. M. Bruaset, and O. Lysne, editors, Simula Research Laboratory - by thinking constantly about it, chapter 22, pages 287–319. Springer, Heidelberg, 2009.

[3] R.E. Klabunde *Electric activity of the heart - Cardiovascular physiology concepts.* Lippincott Williams and Wilkins, Philadelphia, USA, 2005.

[4] L.C. Evans *Partial Differential Equations.* American Mathematical Society, Rhode Island, USA, 1998.

[5] K.D. Joshi *Introduction to General Topology.* New Age International Ltd., New Dehli, India, 1983.

[6] H.H. Sohrab *Basic Real Analysis.* Birkhauser, Boston, USA, 2003.

[7] E.W. Cheney *Introduction to approximation theory.* American Mathematical Society, USA, 1966.

[8] B.P. Rynne and M.A. Youngson *Linear functional analysis.* Springer Verlag, London, UK 2008.

[9] B.F Nielsen, X. Cai and M. Lysaker *On the possibility for computing the transmembrane potential in the heart with a one shot method: An inverse problem.* Mathematical Biosciences 210 (2) (2007) 2008.

[10] J. Serrin *A symmetry theorem in potential theory.* Arch. Rat. Mech. Anal 1971.

[11] S.G. Johnson *Notes on Green's functions in inhomogeneous media.* MIT 2010.

[12] P. Wolfe *Convergence conditions for ascent methods.* Siam Rev 1969

[13] J.E. Dennis and R.B. Schnabel *Numerical Methods for Unconstrained Optimization and Nonlinear Equations.* Siam Publications, Philidelphia 1996

[14] G. Chavent *Nonlinear Least Squares for Inverse Problems.* Springer Dordrecht Heidelberg London New York 2009

[15] Messinger-Rapport, B. J. and Rudy, Y *Regularization of the inverse problem in electrocardiography: A model study* Math Biosci 89:79–118, 1988

[16] Rudy, Y. and Messinger-Rapport, B. J *The inverse solution in electrocardiography: Solutions in terms of epicardial potentials* CRC Crit Rev Biomed Eng, 1988

[17] Gulrajani, R. M., Savard, P., and Roberge, F. A. *The inverse problem in electrocardiography: Solutions in terms of equivalent sources* CRC Crit Rev Biomed Eng, 1988

[18] Gulrajani, R. M. *Models of the electrical activity of the heart and the computer simulation of the electrocardiogram* CRC Crit Rev Biomed Eng, 1988

[19] Gulrajani, R. M., Roberge, F. A., and Mailloux, G. E. *The forward problem of electrocardiography* Comprehensive Electrocardiology. Pergamon Press, Oxford, England, 1989.

[20] Gulrajani, R. M., Roberge, F. A., and Savard, P. *The inverse problem of electrocardiography* Comprehensive Electrocardiology. Pergamon Press, Oxford, England, 1989.

[21] MacLeod, R. S. and Brooks, D. H. *Recent progress in inverse problems in electrocardiology* IEEE Engineering in Medicine and Biology, vol. 17, 1, 1998.

[22] Marieb, E. N. and Hoehn, K *Human anatomy and physiology, 8th ed* Benjamin-Cummings Publishing Company, 2009

[23] Boron, W. F. and Boulpaep, E. L *Midical Physiology - A cellular and molecular approach, 2nd ed* Saunders Elsevier, Philidelphia, USA, 2009

[24] Sundnes, J., Lines, G.T., Cai, X., Nielsen, B.F., Mardal, K.-A., Tveito, A. *Computing the Electrical Activity in the Heart* Springer-Verlag, 2006

[25] Renardy, M. and Rogers, R. C. *An introduction to partial differential equations.* Springer-Verlag, New York, 2004

[26] Nocedal, J. and Wright, S. J. *Numerical Optimization.* Springer Science+Business Media, LLC. USA, 2006

[27] Schmitt, O. H. *Biological information processing using the concept of interpenetrating domains* Information Processing in the Nervous System, KN Leibovic, Ed. New York: Springer-Verlag, 1969

[28] Tung, L. *A bidomain model for describing ischemic myocardial dc potentials* Ph.D. dissertation, Massachusetts Institute of Technolology, Cambridge, 1978

A Small proofs left out in the text

1. Continuous linear operators are Lipschitz continuous - From e.g [8], we have equivalence between continuity and boundedness for linear operators. Hence, let X and Y we normed spaces, and let $T : X \longmapsto Y$ be linear and bounded. Then L is Lipschitz.

Proof:

$$\|Tx - Ty\| = \|T(x-y)\| \leq M\|x-y\|, \quad \forall x, y \in X, \tag{A.1}$$

where M is a constant.

2. Composition of Lipschitz continuous operators are Lipschitz continuous - Let X, Y and Z be normed spaces. Let $T_1 : X \longmapsto Y$ and $T_2 : Y \longmapsto Z$ be two linear, bounded operators. Then $T_2 \circ T_1$ is Lipschitz continuous.

Proof:

$$\begin{aligned} \|T_2(T_1x) - T_2(T_1y)\|_Z = \|T_2(T_1x - T_1y)\|_Z \leq M_2\|T_1x - T_1y\|_Y \\ = M_2\|T_1(x-y)\|_Y \leq M_1M_2\|x-y\|_X. \end{aligned} \tag{A.2}$$

Hence the composition is Lipschitz continuous.

3. Equivalence between bilinear form and minimization problem Let V be a Hilbert space with inner product $(\cdot,\cdot)_V$ and norm $\|\cdot\|_V$. Suppose that the bilinear form a is symmetric and positive semidefinite. Then the abstract variational problem

$$a(u,v) = L(v), \ \forall v \in V, \tag{A.3}$$

is equivalent to the minimization problem $\min_v \in V = F(v)$ for

$$F(v) = \frac{1}{2}a(v,v) - L(v). \tag{A.4}$$

Proof: $\Rightarrow)$: Assume that $a(u,v) = L(v), \ \forall v \in V$. Further, let $w \in V$. Then we have

$$0 = a(u, u-w) - L(u-w) = a(u,u) - a(u,w) - L(u,w). \tag{A.5}$$

Now, we claim that $a(u,w) \leq \frac{1}{2}a(u,u) + \frac{1}{2}a(w,w)$. This follows from

$$0 \leq a(u-w, u-w) = a(u-w, u) - a(u-w, w)$$
$$= a(u,u) - a(w,u) - a(u,w) + a(w,w) = a(u,u) - 2a(u,w) + a(w,w).$$

Thus, the claim follows, and we get that

$$0 \leq a(u,u) - \frac{1}{2}a(u,u) - \frac{1}{2}a(w,w) - L(u) + L(w). \tag{A.6}$$

Hence,

$$\frac{1}{2}a(w,w) - L(w) \geq \frac{1}{2}a(u,u) - L(u), \ \forall w \in V. \tag{A.7}$$

$\Leftarrow$) : Assume that u satisfies $\min_{v \in V} F(v)$. Let $v \in V$ and $\epsilon \in \mathbb{R}$. Define $g : \mathbb{R} \longmapsto \mathbb{R}$ by

$$g(\epsilon) = \frac{1}{2}a(u+\epsilon v, u+\epsilon v) - L(u+\epsilon v). \tag{A.8}$$

Since u is the minimizer, then clearly $g(0) \leq g(\epsilon)$, so it follows that $g'(0) = 0$. Hence, it follows by the chain rule that

$$g'(0) = \frac{1}{2}a(v,u) + \frac{1}{2}a(u,v) - L(v) = 0 \Rightarrow a(u,v) - L(v) = 0$$
$$\Rightarrow a(u,v) = L(v). \tag{A.9}$$

4. Equivalent inner product - Let H be a Hilbert space. Then will a symmetric, continuous, coercive bilinear operator $a(\cdot,\cdot) : H \times H \longmapsto \mathbb{R}$ introduce a equivalent inner product on H.

Proof: Let $x, y, z \in H$ and $\alpha, \beta \in \mathbb{R}$. A real inner product satisfy the four following properties:

$$\begin{aligned} (i) &\quad (x,x) \geq 0 \\ (ii) &\quad (x,x) = 0 \text{ if and only if } x = 0 \\ (iii) &\quad (\alpha x + \beta y, z) = \alpha(x,z) + \beta(y,z) \\ (iv) &\quad (x,y) = (y,x). \end{aligned}$$

From the symmetry property, property (iv) is clearly satisfied. Also, from the bilinearity, (iii) is satisfied. Further, let $u \in H$ be arbitrary. The coercivity property states that

$$\|u\|_H^2 \leq \alpha \ a(u,u), \tag{A.10}$$

for some constant $\alpha > 0$. Hence, $a(u,u) > 0$ for all $u \neq 0$. To show that $a(u,u) = 0$ when $u = 0$, we use the continuity property, which says that

$$|a(u,v)| \leq C\|u\|_H\|v\|_H, \quad \forall u,v \in H. \tag{A.11}$$

Hence,

$$|a(u,u)| \leq C\|u\|_H^2, \tag{A.12}$$

which concludes the proof.

5. Continuity of least-squares operator - Let $F : \mathbb{R}^n \longmapsto L^2(\partial B)$ be continuous, where $B \subset \mathbb{R}^m$. Then the operator $G : \mathbb{R}^n \longmapsto \mathbb{R}$ defined by

$$G(x) = \frac{1}{2}\int_{\partial B}(F(x) - d)^2 \; dS, \tag{A.13}$$

is continuous as well.

Proof: Since F is continuous, we know that for an arbitrary $x \in \mathbb{R}^n$, there will for any $\epsilon > 0$ exists a $\delta > 0$ such that $\|F(x) - F(y)\|_{L^2(\partial B)} < \epsilon$ whenever $\|x - y\|_{\mathbb{R}^n} < \delta$.

Hence, if we let let $x, y \in \mathbb{R}^n$ such that $\|F(x) - F(y)\|_{L^2(\partial B)} < \epsilon_1$, then

$$\begin{aligned}
|G(x) - G(y)| &= \frac{1}{2}\left|\int_{\partial B}(F(x) - d)^2 - (F(y) - d)^2 \; dS\right| \\
&= \frac{1}{2}\left|\int_{\partial B} F^2(x) - 2dF(x) - F^2(y) + 2dF(y) \; dS\right| \\
&\leq d\int_{\partial B}|F(x) - F(y)| \; dS + \frac{1}{2}\int_{\partial B}|F^2(x) - F^2(y)| \; dS \\
&= d\int_{\partial B}|F(x) - F(y)| \; dS + \frac{1}{2}\int_{\partial B}|F(x) - F(y)||F(x) + F(y)| \; dS \\
&\leq C\left(\int_{\partial B}|F(x) - F(y)|^2 \; dS\right)^{1/2} \\
&= C\|F(x) - F(y)\|_{L^2(\partial B)} < C\epsilon_1 = \epsilon,
\end{aligned} \tag{A.14}$$

whenever $\|x - y\|_{\mathbb{R}^n} < \delta$.